Altered organisation of the intermediate filament cytoskeleton and relocalisation of proteostasis modulators in cells lacking the ataxia protein sacsin

Emma J. Duncan[1], Roxanne Larivière[2], Teisha Y. Bradshaw[1], Fabiana Longo[3,4], Nicolas Sgarioto[2] Matthew J. Hayes[5], Lisa E.L. Romano[1], Suran Nethisinghe[1], Paola Giunti[6], Michaela B. Bruntraeger[1], Heather D. Durham[7], Bernard Brais[2], Francesca Maltecca[3], Benoit J. Gentil[7] and J. Paul Chapple[1]

[1] William Harvey Research Institute, Barts and the London School of Medicine, Queen Mary University of London, London, EC1M 6BQ, United Kingdom.

[2] Department of Neurology and Neurosurgery, Montreal Neurological Institute, McGill University, Montreal, QC, Canada H3A 2B4.

[3] Università Vita-Salute San Raffaele and Division of Genetics and Cell Biology, San Raffaele Scientific Institute, Milan, Italy

[4.] Università degli Studi dell'Insubria, Italy.

[5] UCL Institute of Ophthalmology, 11-43 Bath Street, London, EC1V 9E, United Kingdom.

[6] Department of Molecular Neuroscience, UCL Institute of Neurology, London, WC1N 3BG, United Kingdom.

[7] Laboratory of Neurogenetics of Motion, Montreal Neurological Institute, McGill University, Montreal, QC, Canada H3A 2B4.

Address for correspondence:

Professor Paul Chapple
Centre for Endocrinology
William Harvey Research Institute
Barts and the London School of Medicine
Queen Mary University of London
Charterhouse Square
London EC1M 6BQ
United Kingdom
Tel: +44 20 7882 6242
Email: j.p.chapple@qmul.ac.uk

Abstract

Autosomal Recessive Spastic Ataxia of Charlevoix-Saguenay (ARSACS) is caused by mutations in the gene *SACS*, encoding the 520 kDa protein sacsin. Although sacsin's physiological role is largely unknown, its sequence domains suggest a molecular chaperone or protein quality control function. Consequences of its loss include neurofilament network abnormalities, specifically accumulation and bundling of perikaryal and dendritic neurofilaments.

To investigate if loss of sacsin affects intermediate filaments more generally, the distribution of vimentin was analysed in ARSACS patient fibroblasts and in cells where sacsin expression was reduced. Abnormal perinuclear accumulation of vimentin filaments, which sometimes had a cage-like appearance, occurred in sacsin-deficient cells. Mitochondria and other organelles were displaced to the periphery of vimentin accumulations.

Reorganisation of the vimentin network occurs *in vitro* under stress conditions, including when misfolded proteins accumulate. In ARSACS patient fibroblasts HSP70, ubiquitin and the autophagy-lysosome pathway proteins Lamp2 and p62 relocalised to the area of the vimentin accumulation. There was no overall increase in ubiquitinated proteins, suggesting the ubiquitin proteasome system was not impaired. There was evidence for alterations in the autophagy-lysosome pathway. Specifically, in ARSACS HDFs cellular levels of Lamp2 were elevated while levels of p62, which is degraded in autophagy, were decreased. Moreover, autophagic flux was increased in ARSACS HDFs under starvation conditions.

These data show that loss of sacsin effects the organisation of intermediate filaments in multiple cell types, which impacts the cellular distribution of other organelles and influences autophagic activity.

Introduction

Autosomal Recessive Spastic Ataxia of Charlevoix-Saguenay (ARSACS) is a neurodegenerative disease associated with progressive loss of Purkinje neurons [1, 2]. It is a childhood onset condition that is characterised by cerebellar ataxia, pyramidal spasticity and peripheral neuropathy. At the genetic level, ARSACS is caused by mutations in the *SACS* gene [3]. This encodes the extremely large (4579 amino acid) modular protein sacsin, which from its N- to C-terminus is composed of a ubiquitin-like domain that binds to the proteasome [4], three large sacsin repeat regions (SRR) that may have an Hsp90-like function [5, 6], a J-domain that binds HSP70 [4, 5] and a higher eukaryotes and prokaryotes nucleotide-binding (HEPN) domain that can dimerise [7]. Based on the presence of these conserved domains, some of which are present in molecular chaperones and components of the ubiquitin proteasome system, it is a possibility that sacsin may function in proteostasis.

It is unclear if a molecular chaperone role for sacsin would be consistent with findings from cellular and mouse models of ARSACS, where cytoskeletal and mitochondrial abnormalities have been identified. Specifically, in the *Sacs*$^{-/-}$ mouse we have shown that loss of sacsin results in abnormal neurofilament accumulations in the somatodendritic regions of several neuronal populations as early as 14 days after birth [8]. Furthermore, in cultured hippocampal neurons where sacsin was targeted with shRNA, and in spinal motor neurons and dorsal root ganglion neurons cultured from *Sacs*$^{-/-}$ mice, a similar redistribution of neurofilament was observed. These abnormal neurofilament accumulations were demonstrated to contain the hypo-phosphorylated form of neurofilament heavy chain protein (NFH) [8]. In addition to intermediate filament defects, loss of sacsin altered mitochondrial morphology, dynamics and distribution. Mitochondrial length is increased [2, 8, 9], consistent with reduced mitochondrial recruitment of the fission factor dynamin related protein 1 (Drp1) contributing to this phenotype [9]. In agreement with others, we have also demonstrated that the morphological alterations in mitochondrial networks are accompanied by impaired oxidative phosphorylation and increased oxidative stress [2, 9, 10]. Mitochondrial motility was impaired in motor neurons cultured from *Sacs*$^{-/-}$ mice [8]. Together these data indicate that loss of sacsin causes problems with both the intermediate filament cytoskeleton and mitochondria function, phenotypic aspects that are not mutually exclusive given the importance of the cytoskeleton in regulating mitochondrial dynamics [11, 12].

As we had observed impaired mitochondrial function in human dermal fibroblasts (HDFs) from ARSACS patients [2, 9, 10], we hypothesised that these cells may also exhibit cytoskeletal changes. Thus, we investigated the organisation of the vimentin intermediate filament network in human dermal fibroblasts (HDF) derived from skin biopsies of ARSACS patients (vimentin being the major intermediate filament protein in fibroblasts). In a proportion of ARSACS cells,

intermediate filaments were bundled and collapsed as a cage-like structure around the microtubule organising centre (MTOC) rather than radiating from the nucleus towards the plasma membrane, as in control cells. These vimentin structures were reminiscent of the ‘cage’ of the vimentin intermediate filaments that surround aggresomes. Aggresomes form when misfolded protein aggregates are trafficked in a retrograde manner to the MTOC, where they accumulate prior to clearance by the autophagy-lysosome machinery [13, 14]. Thus, we investigated the distribution and function of the proteostasis machinery in ARSACS fibroblasts, observing components of the cellular proteostasis machinery relocalised within the accumulations of vimentin. Moreover, aspects of the phenotype were recapitulated in primary neurons from the *Sacs*$^{-/-}$ mouse. In combination, our data show that loss of sacsin impacts on intermediate filament organisation leading to changes in the cellular distribution of proteostasis system components and altered autophagy.

Results

The vimentin intermediate filament cytoskeleton is disrupted in ARSACS patient fibroblasts

We primarily report on ARSACS HDF lines from four patients that are compound heterozygous (p.Q4054* & c.2094-2A>C; p.R2002fs & p.Q4054*; p.F2780C & p.S3892*; p.K1715* & p.R4331Q) and one patient that is homozygous (p.2801delQ) (Figure S1A). Cell lines from two further compound heterozygous patients, sharing two variants in cis on one allele (p.R3636Q:p.P3652T) and a different frameshift on the other allele (p.L3745Rfs or p.C72Cfs) [15], plus two patients homozygous for the 8844delT mutation, the major founder mutation in Québec, were also investigated (Figures S1C, D). Using an antibody directed to the C-terminus of sacsin, immunoblot showed that levels of the protein were similar in control HDFs and the HDF line with the p.2801delQ mutation. Some sacsin was also detected in HDFs from the ARSACS patient with the p.R3636Q:p.P3652T:p.C72Cfs mutations (Figure S1). Sacsin was not conclusively detected in cell lines from patients with the other mutations investigated.

Confocal imaging revealed that a large proportion of cells in all of the ARSACS patients HDF lines investigated had a grossly abnormal vimentin cytoskeleton. In contrast to wild-type control cells, where vimentin was distributed throughout the cytoplasm, vimentin filaments were bundled in perinuclear accumulations in patient cells (Figure 1A, B and S2). This phenotype was highly penetrant with 79.6±1.9% of ARSACS HDFs (Figure 1B and S2A) having a disorganised vimentin network, relative to just 8.5±1.2% of control cells. Vimentin filaments were also disrupted in the ARSACS lines that still have detectable sacsin protein, with sacsin being localised to the area of filament accumulation, rather than being distributed throughout the cytoplasm in wild-type control cells (Figure 1C).

Transmission electron microscopy (TEM) revealed that in ARSACS HDFs cytoplasmic organelles were localised peripherally to a perinuclear region of uniform electron density (Figure 1D). Higher magnification imaging indicated this region contained significant amounts of approximately 10 nm filamentous material, consistent with the size of intermediate filaments. The region of filamentous material accumulation frequently contained vesicular structures and vacuoles.

Sacsin knockdown disrupts vimentin intermediate filament organisation in wild-type cells

To further confirm that loss of functional sacsin results in altered vimentin organisation, siRNA-mediated knockdown was used to deplete sacsin in wild-type HDFs, using previously validated siRNAs [4, 9] A significant increase ($p<0.01$) in the percentage of sacsin knockdown HDFs that exhibited a perinuclear accumulation of vimentin was observed relative to controls, with vimentin bundles visible in some cells (Figure 2A). We also made a HEK293 sacsin knockout line using CRISPR/Cas9 genome editing. These cells did not express detectable levels of sacsin and also

exhibited perinuclear collapse of the vimentin network (Figure 2B, C). In these cells, we were able to rescue the vimentin phenotype by transfection of a plasmid for expression of full-length sacsin-GFP (Figure 2B, C).

Vimentin accumulates around the MTOC and disrupts the distribution of organelles in ARSACS patient cells

As cytoskeletal elements are interlinked we used confocal analyses to investigate if the actin filament and microtubule networks were disrupted in ARSACS HDFs. We observed no gross abnormalities in actin microfilament (not shown) or microtubule organisation. However, labelling with anti-tubulin did reveal that the abnormal accumulations of vimentin formed in close proximity to the MTOC (Figure 3A and S3A).

Collapse of the vimentin network would be expected to have consequences for the distribution of organelles, as the cytoskeleton organises the intracellular space. Indeed, confocal imaging showed displacement of mitochondria to areas peripheral to the abnormal accumulations of vimentin in ARSACS patient cells (Figure 1A). Disruption of the intermediate filament cytoskeleton has also been reported to interfere with Golgi organisation [16, 17]. Confocal imaging of HDFs immunolabeled with the Golgi protein, GS28, revealed a fragmented Golgi stack, with cisternae displaced around an area of cytoplasm where mitochondria where also absent (Figure 3B and S3B). With available antibodies, it was not possible to double-label cells with antibodies to vimentin and GS28, but it is likely that fragmented Golgi was displaced around areas of vimentin accumulation. Distribution of the endosome marker, EEA1, was also altered in ARSACS HDFs. Relative to wild-type controls, endosomes were less evenly distributed throughout the cell (Figure S3C), distributing with displaced mitochondria.

Components of the cellular proteostasis machinery relocalise to the region of abnormal vimentin accumulation in ARSACS patient cells

The combination of perinuclear accumulation of vimentin around the MTOC, disrupted mitochondrial network organisation and Golgi fragmentation have been linked to aggresome formation in cultured cells. Aggresomes are juxtanuclear accumulations of misfolded proteins that form through a regulated process when cellular protein-degradation systems become overwhelmed, a common phenomenon in neurodegenerative disorders [18-20]. To look for evidence of disrupted proteostasis in ARSACS HDFs, cells were immunolabeled with an antibody that detects both constitutive (HSPA8) and inducible (HSPA1) isoforms of the molecular chaperone HSP70, which interacts with misfolded proteins and can localise to aggresomes [21, 22]. In control HDFs, HSP70 labelling was distributed throughout the cytoplasm, while in patient cells HSP70 was frequently enriched in the region with abnormal accumulation of vimentin (Figure 4A and Figure S4A). Confocal z-stack images indicated HSP70 was surrounded by a ‘cage-like’ bundle of

vimentin, with some HSP70 also interspersed within the abnormal accumulation of vimentin. HSP70 labelling appeared reduced in other regions of the cytoplasm. This relocalisation of HSP70 in ARSACS HDFs was not accompanied by an increase in overall cellular levels of HSPA8 or expression of HSPA1, as determined by immunoblot (Figure 4E, F).

Misfolded proteins that cannot be refolded by chaperones are normally targeted for degradation by ubiquitination. Thus, we next compared localisation of ubiquitin in wild-type and ARSACS HDFs. Similar to HSP70, we observed ARSACS HDFs where ubiquitin labelling was redistributed to the area of vimentin accumulations, rather than being dispersed as in control cells (Figure 4B). The percentage of cells with this ubiquitin phenotype (14±3%) was low relative to the those that relocalised HSP70 (85±2%) and there was no significant change in level of ubiquitinated proteins in ARSACS HDFs relative to wild-type HDFs. Immunoblots indicated this was the case, both in cells cultured under normal conditions and in cells treated with MG132 to inhibit proteasome activity (Figure 4G). Together these data indicate that although proteostasis-linked proteins are relocalised in response to loss of sacsin, the ubiquitin-proteasome system does not appear compromised.

Lamp2 and other components of the autophagy-lysosome pathway are relocalised to the region of abnormal vimentin accumulation in ARSACS patient cells and have altered cellular levels

Separate to aggresome formation, vimentin deficiency is associated with juxtanuclear accumulation of lysosomes [23]. To ascertain if lysosome localisation was altered in ARSACS HDFs, control and patient cells were immunolabeled for vimentin and lysosomal-associated membrane protein 2 (Lamp2). Lamp2 was distributed throughout the cytoplasm in control HDFs. In a significant ($p<0.01$) percentage of patient cells Lamp2 positive puncta were clustered within the region of vimentin accumulation, here it was both interspersed with the vimentin and localised within the vimentin 'cage' (Figure 5A, C band S5). Similar to Lamp2, the ubiquitin-binding autophagic adaptor protein p62 (also known as SQSTM1), which is required for autophagic clearance of ubiquitinated proteins [24, 25], was also relocalised within the vimentin cage (Figure 5B, D). Immunoblot showed a small, but statistically significant, increase in Lamp2 levels in ARSACS HDF relative to controls (1.19-fold increase, $p<0.05$) (Figure 5E, F). Contrastingly, levels of p62 were reduced in ARSACS HDFs relative to controls (0.5-fold decrease, $p<0.05$). This was of particular interest as p62 has been identified as one of the specific substrates that is degraded through the autophagy-lysosome pathway [26-28].

Autophagic flux is altered in ARSACS patient cells

We next considered whether autophagosomes accumulated in the region of the vimentin cage. Ultrastructural analyses of ARSACS patient cells reveals accumulation of filamentous material are

interspersed with components of the autophagy-lysosome system, including autophagosomes (Figure 6A). The presence of autophagosomes within the filament accumulations and the immunolabeling of lysosomes within the vimentin 'cage' (Figure 5A) are consistent with autophagic clearance happening at this location.

To ascertain if there was increased activation of the autophagy-lysosome pathway in ARSACS HDFs, the number of LC3 positive puncta were quantified from confocal images of immuolabeled patient and control cells (Figure 6B, C). The number of LC3 positive puncta was not significantly different between ARSACS HDFs and control cells under basal conditions. In contrast, induction of autophagy by nutrient starvation only resulted in an increase in LC3 positive puncta in control cells ($p<0.001$). This indicates that either LC3 positive puncta are not forming in response to nutrient starvation in ARSACS HDFs or their turnover is increased. Since generation of LC3-II from its precursor, LC3-I, correlates with autophagosome formation, levels of LC3-I and LC3-II were assessed by immunoblotting (Figure 6D, E). Under basal conditions, levels of LC3-I were similar in ARSACS patient and controls, but LC3-II was not detectable at quantifiable levels. When autophagy was induced by nutrient starvation LC3-II levels increased in starved cells, and importantly, significantly more LC3-II accumulated in controls than patient cells. To understand why less LC3-II accumulated in ARSACS HDFs relative to controls, we inhibited lysosomal degradation using bafilomycin A. In nutrient starved cells treated with bafilomycin A, levels of LC3-II were not significantly different between ARSACS and control HDFs. The same result was observed when autophagy was inhibited with 3-Methyladenine (Figure 6D, E). These data suggest that LC3 is more rapidly degraded and that autophagic flux is increased under conditions that induce autophagy in ARSACS HDFs.

Neurofilament bundling, organelle displacement and relocalisation of ubiquitin occurs in *Sacs*$^{-/-}$ primary neurons

We previously reported abnormal bundling of neurofilaments in primary spinal motor and sensory neurons cultured from *Sacs*$^{-/-}$ mouse embryos [8]. In 4-week-old dissociated spinal cord cultures, bundling of neurofilaments was detected in the soma of *Sacs*$^{-/-}$ motor (85.4±4.9%) and sensory neurons (73.5±8.5%) by immunolabeling with antibody against the high molecular weight neurofilament protein (NFH), as previously described [8] (Figure 7A). In motor neurons, the normal neurofilament network courses through the cell body into the dendritic processes, whereas dorsal root ganglion (DRG) sensory neurons lack dendrites. In *Sacs*$^{-/-}$ motor neurons, neurofilaments coalesce into linear bundles, whereas in DRG neurons, they can form a juxtanuclear ball reminiscent of vimentin bundles in fibroblasts. Peripheral displacement of the nucleus was particularly visible in DRG sensory neurons with a collapsed neurofilament network (Figure 7B, C). Mitochondria were excluded from the region of the neurofilament accumulations (Figure 7D). Moreover, ubiquitin had a more perinuclear distribution in *Sacs*$^{-/-}$ neurons compared to controls

(Figure 7G, H); this was statistically significant in both motor neurons ($p<0.05$) and DRG sensory neurons ($p<0.05$) (Figure 7E, H). In contrast to ARSACS patient HDFs, there was no significant redistribution of the autophagy-lysosomal proteins Lamp2 or p62 in *Sacs*$^{-/-}$ neurons (not shown).

Discussion

Here we present evidence that organisation of the vimentin cytoskeleton is dramatically altered in ARSACS HDFs with a range of sacsin mutations and in cellular models where sacsin has been depleted. This is in agreement with our previous findings that abnormal accumulations of neurofilament occur in *Sacs*$^{-/-}$ primary neurons [8]. Importantly, these data indicate that loss of sacsin impacts on more than one type of intermediate filament, suggesting sacsin function may be broadly required for normal intermediate filament organisation.

Cells lacking functional sacsin also exhibit abnormalities in organelle distribution, such as fragmentation of the Golgi in ARSACS HDFs and asymmetrical positioning of nuclei in *Sacs*$^{-/-}$ neurons. This is consistent with intermediate filaments playing a role in intracellular organelle distribution [29, 30] and may be relevant to the pathogenesis of ARSACS. We have previously shown recruitment of the fission factor Drp1 to mitochondria is impaired in sacsin null cells, proposing this partly explains the alterations in mitochondrial dynamics and function observed in cellular models of ARSACS [9]. Displacement of mitochondria at the periphery of vimentin accumulations in ARSACS HDFs suggests that disrupted organelle distribution may also impact mitochondrial network organisation and potentially function. Interestingly, in HDFs transiently transfected with siRNA targeting sacsin, there was not an obvious alteration in mitochondrial localisation compared to that which we observed in ARSACS patient HDFs. We speculate that this difference is likely due to partial knockdown of sacsin and/or that the time after transfection (48 hours) was not sufficient to induce this aspect of the loss of sacsin phenotype.

Collapse of the vimentin network around the MTOC occurs when mechanisms regulating intermediate filaments are disrupted and as well as in response to stress conditions such as the accumulation of misfolded protein aggregates [18, 23, 31]. We did not see any direct evidence for accumulation of protein aggregates in ARSACS patient HDFs by TEM, or find the UPS to be compromised (i.e. no accumulation of ubiquitinated proteins). This suggests that the altered vimentin network in sacsin deficient cells is not the result of a problem with clearance of ubiquitinated proteins. Although ubiquitinated proteins did not accumulate in ARSACS HDFs, multiple components of the proteostasis machinery were relocalised to the pericentriolar region of vimentin accumulation. These included HSP70 and components of the autophagy-lysosome machinery. Interestingly, levels of p62 were decreased in ARSACS fibroblasts, while Lamp2 levels were elevated. p62 is degraded by autophagy and Lamp2 promotes fusion of autophagosomes with lysosomes [28, 32]. We analysed LC3 levels to determine if autophagy was activated in ARSACS HDFs, demonstrating autophagic flux was increased under conditions of nutrient starvation. These data suggest that the relocalisation of lysosomes in ARSACS HDFs is associated with functional changes in the autophagy-lysosome pathways. This would be in

agreement with juxtanuclear clustering of lysosomes being associated with increased autophagosome-lysosome fusion rates [33, 34].

The phenotypes observed in ARSACS HDF and primary neurons from the *Sacs*$^{-/-}$ mouse only partially recapitulated each other. For example, while vimentin is organised as a 'cage' in some ARSACS HDFs, neurofilaments form bundles, especially in dendrites, reflecting a difference in the organisation of the cytoarchitecture. Moreover, we did not see any evidence for relocalisation of components of the autophagy-lysosomes pathway in primary neurons from the *Sacs*$^{-/-}$ mouse, but did see perinuclear accumulation of ubiquitin in neurons from the *Sacs*$^{-/-}$ mouse. This ubiquitin staining may represent ubiquitinated proteins that are destined for removal by the autophagy-lysosome pathway, although we did not see any evidence for relocalisation of lysosomes or autophagy proteins in primary neurons. These differences between neurons and fibroblasts may reflect cell-specific aspects of cytoskeleton or proteostasis regulation. Indeed, previous reports show that common inducers of autophagy in non-neuronal cells fail to stimulate autophagy in primary neurons, highlighting that autophagy in neurons is regulated by mechanisms that may differ from those in non-neuronal cells [35, 36].

The sequence of events that lead to neuronal cell death in ARSACS is unknown but most of the evidence supports that the cytoskeletal disorganisation is an early phenomenon [8]. Altered proteostasis, mitochondrial dysfunction and cytoskeletal abnormalities are all features observed in other neurodegenerative diseases. These components of molecular pathology frequently occur in combination with multiple complex links between them. For ARSACS, based on the presence of domains linking to molecular chaperones and the UPS it would be reasonable to speculate sacsin has a role in protein quality control, most likely for a specific client or family of client proteins. If this is the case it would suggest that loss of sacsin function would result in altered levels or function of these clients at an early stage in the molecular pathogenesis of the disease. Our data may suggest that these clients will be linked to proteins involved in regulation of intermediate filaments or could even be intermediate filament proteins.

In conclusion, this study shows that loss of sacsin effects organisation of intermediate filament networks with consequences for intracellular architecture. In fibroblasts, these include repositioning of components of the autophagy-lysosome pathway and subsequent alterations of autophagic activity.

Materials and Methods

Cell culture and sacsin knockdown

ARSACS patient fibroblasts were a gift from Dr Sascha Vermeer at Radboud University Nijmegen Medical Centre (Nijmegen, Netherlands) and Dr Paola Giunti at UCL Institute of Neurology (London, UK). The cells were collected as part of a project approved by the Medical Ethics Committee of the Radboud University (CMO-nr 2014/155), and Giunti has ethical approval for dermal fibroblast collection through a European integrated project on spinocerebellar ataxias (REC Ref - 04/Q0505/21). Written informed consent to participate in this study was obtained from all patients. Control and ARSACS HDF lines used in this work were not closely age or sex matched, but were all between passage 3 and 8. HDFs were cultured in DMEM supplemented with 10% FBS and 50U/ml penicillin and 50µg ml^{-1} streptomycin (final concentration in media 1%). All cells were kept in a constant humidified atmosphere of 5% CO_2 at 37ºC. Cell culture reagents were from Life Technologies (Paisley, UK).

SH-SY5Y cells were from the American Type Culture Collection and were grown in Dulbecco's Minimum Eagle Medium (DMEM) at a 1:1 ratio with Ham's F12 medium. Cells were maintained in medium supplemented with 10% heat-inactivated foetal bovine serum (FCS) containing 100U ml^{-1} penicillin and 100 mg ml-1 streptomycin.

For sacsin knockdown, a combination of three previously validated siRNAs targeting exons 7 (sense: GGAUGAUCCUCUGAAGGUC), 8 (sense: GCGGCCGAAUUCUAUAAAG) and 10 (sense: CGUAAGAUUUCUAGAUGAC) of *SACS* were used [2, 4]. These siRNAs were at a concentration of 10nM each and were transfected in combination using Lipofectamine 3000 (ThermoFisher Scientific, UK), according to the manufacturer's instructions. A negative control siRNA that has no significant sequence similarity to human gene sequences was used as a control at a concentration of 30nM.

Generation of CRISPR/Cas9 *SACS*$^{-/-}$ Flp-In T-REx HEK293 cells was performed following the manufacturers protocol for the sacsin double nickase plasmid (SantaCruz Biotechnology, cat. no. sc-404592-NIC). For inhibition of the proteasome MG132 was added to cells at a final concentration of 10µm for 3 hours. For inhibition of autophagy, Bafilomycin was added to cells at a concentration of 100nm for 3 hours and 3-MA at a concentration of 5mM for 3 hours.

Sacs$^{-/-}$ primary neurons were cultured from the *Sacs*$^{-/-}$ mouse as described previously [2, 8].

Immunofluorescent detection and staining

Immunofluorescent labeling was as described previously [2]. Briefly, cells cultured on glass coverslips were fixed with 4% formaldehyde for 15 minutes and then permeablised for 5 minutes

with 0.2% Triton-X 100. Cells were incubated with primary antibodies for 2 hours in 0.02% Triton-X100, 1% bovine serum albumin and 10% normal goat serum, prior to washing and incubation with fluorescently labelled secondary antibodies (Alexa Fluor 488-conjugated goat anti-rabbit or anti-mouse, Alexa Fluor 543 conjugated goat anti-mouse or anti-rabbit, or Alexa Fluor 647-conjugated goat anti-mouse or anti-rabbit (ThermoFisher Scientific). Cells were then counterstained with DAPI and coverslips mounted for microscopy. Primary antibodies were used at the following titres; 1:100 for rabbit monoclonal anti-vimentin (Abcam, UK), 1:100 for mouse monoclonal anti-vimentin (Abcam), 1:100 for rabbit monoclonal anti-sacsin (Abcam), 1:500 for mouse monoclonal anti-GS28 (Enzo Life Sciences, UK), 1:100 for mouse monoclonal anti-EEA1 (BD Biosciences, UK), 1:100 for mouse monoclonal anti-HSP70 (Sigma, Poole, UK), 1:100 for rabbit polyclonal anti-ubiquitin (Abcam), 1:100 for mouse monoclonal anti-Lamp2 (Santa Cruz, USA), 1:100 for mouse monoclonal anti-p62 (Abcam) and 1:100 for rabbit polyclonal anti-LC3 (Abcam). For staining of mitochondria with MitoTracker (ThermoFisher Scientific) the stock solution was diluted to a concentration of 100nM in cell culture media prior to addition to cells for 30 minutes at 37ºC in 5% CO_2 atmosphere. After the incubation period, cells were washed twice in cell culture media prior to live imaging or fixation. Confocal microscopy was performed using a LSM510 or an LSM880 (Zeiss) with a 63x objective. Quantification of incidence of cells with perinuclear localisation of HSP70, ubiquitin, Lamp2 and p62 was performed blind to experimental status. Incidence of LC3 punctae were quantified from confocal Z-stacks using a combination of the Surpass module and MeasurementPro modules of Imaris (Imaris 7.6.1 Bitplane, Concord, USA). Surface rendered 3D images were generated, with thresholding for punctae size and intensity consistent between images and experimental conditions.

Immunoblotting

Proteins were size-fractionated using precast 4-12% gradient NuPAGE Bis-Tris gels (Life Technologies) and transferred to nitrocellulose membranes (Whatman). Membranes were blocked in either 5% (w/v) non-fat milk powder or 5% (w/v) bovine serum albumin (BSA) before probing with the specified antibodies. Primary antibodies were used at the following titres; 1:1600 for rabbit monoclonal anti-sacsin (Abcam), 1:5000 for mouse monoclonal anti-HSP70 (Sigma) 1:5000 for mouse monoclonal anti-Lamp2 (Santa Cruz), 1:3000 for rabbit polyclonal anti LC3 (Abcam) 1:10000 for mouse monoclonal anti-β-actin (Sigma), 1:5000 for rabbit polyclonal anti-GAPDH (Abcam), 1:1000 for mouse monoclonal anti-p62 (Abcam), and 1:3000 for rabbit polyclonal anti-LC3 (company). Immunoreactive products were visualised and quantified, after labelling with species-specific infrared secondary antibodies (1:5000, LI-COR Biosciences, UK), using the Odyssey imaging system (LI-COR). Apparent molecular masses were estimated using the Novex Sharp Pre-stained Protein Standard (Life Technologies) or HiMark Pre-stained Protein Standard (Life Technologies) and the band sizing application in Odyssey software (LI-COR Biosciences). Images of the immunoblots were also quantified using the Odyssey software.

Transmission electron microscopy

Cells were grown on glass or Thermanox cover-slips and fixed overnight in cold (4°C) Karnovky's fixative (2% paraformaldehyde and 2.5% glutaraldehyde in 0.08M cacodylate buffer). They were then washed 3 times in phosphate buffer and osmicated with 1% osmium tetroxide in ddH_2O for 1 hour. Samples were then washed 3 x 10 minutes in ddH_2O and dehydrated with a series of alcohols: 30%, 50%, 70%, 90%, 3 x 100% and 2 x propylene oxide (at least 20 minutes in each). They were infiltrated with 50% propylene oxide: 50% araldite resin overnight and with several changes of 100% resin the next day. Resin blocks were cured at 60°C overnight. Sectioning was done using a Leica Ultracut UCT microtome. Sections were counter-stained Reynold's lead citrate and were viewed on a JEOL 1010 TEM (JEOLUSA, USA).

Statistical analyses

All data are expressed as means ± SEM, unless otherwise stated. Statistical significances were determined using Mann-Whitney U tests or unpaired Student's *t*-tests as appropriate.

Acknowledgments

This work was supported by BBSRC [BB/L02294X/1]; the CIHR Rare Disease Emerging Team grant, the Ataxia of Charlevoix-Saguenay Foundation; Muscular Dystrophy Canada and Barts and the London Charity [417/1699]. The LSM880 confocal used in these studies was purchased through a Barts and the London Charity grant MGU0293. We thank prof. P. De Jonghe and his group, VIB-University of Antwerp, Belgium, for providing us with the skin biopsies of R3636Q:P3652T/L3745Rfs and R3636Q:P3652T/C72Cfs patients.

References

1. Bouhlal Y, Amouri R, El Euch-Fayeche G, Hentati F: **Autosomal recessive spastic ataxia of Charlevoix-Saguenay: an overview**. *Parkinsonism Relat Disord* 2011, **17**(6):418-422.
2. Girard M, Lariviere R, Parfitt DA, Deane EC, Gaudet R, Nossova N, Blondeau F, Prenosil G, Vermeulen EG, Duchen MR *et al*: **Mitochondrial dysfunction and Purkinje cell loss in autosomal recessive spastic ataxia of Charlevoix-Saguenay (ARSACS)**. *Proc Natl Acad Sci U S A* 2012, **109**(5):1661-1666.
3. Engert JC, Berube P, Mercier J, Dore C, Lepage P, Ge B, Bouchard JP, Mathieu J, Melancon SB, Schalling M *et al*: **ARSACS, a spastic ataxia common in northeastern Quebec, is caused by mutations in a new gene encoding an 11.5-kb ORF**. *NatGenet* 2000, **24**(2):120-125.
4. Parfitt DA, Michael GJ, Vermeulen EG, Prodromou NV, Webb TR, Gallo JM, Cheetham ME, Nicoll WS, Blatch GL, Chapple JP: **The ataxia protein sacsin is a functional co-chaperone that protects against polyglutamine-expanded ataxin-1**. *HumMolGenet* 2009, **18**(9):1556-1565.
5. Anderson JF, Siller E, Barral JM: **The sacsin repeating region (SRR): a novel Hsp90-related supra-domain associated with neurodegeneration**. *J Mol Biol* 2010, **400**(4):665-674.
6. Anderson JF, Siller E, Barral JM: **The neurodegenerative-disease-related protein sacsin is a molecular chaperone**. *J Mol Biol* 2011, **411**(4):870-880.
7. Kozlov G, Denisov AY, Girard M, Dicaire MJ, Hamlin J, McPherson PS, Brais B, Gehring K: **Structural basis of defects in the sacsin HEPN domain responsible for autosomal recessive spastic ataxia of Charlevoix-Saguenay (ARSACS)**. *J Biol Chem* 2011, **286**(23):20407-20412.
8. Lariviere R, Gaudet R, Gentil BJ, Girard M, Conte TC, Minotti S, Leclerc-Desaulniers K, Gehring K, McKinney RA, Shoubridge EA *et al*: **Sacs knockout mice present pathophysiological defects underlying autosomal recessive spastic ataxia of Charlevoix-Saguenay**. *Hum Mol Genet* 2015, **24**(3):727-739.
9. Bradshaw TY, Romano LE, Duncan EJ, Nethisinghe S, Abeti R, Michael GJ, Giunti P, Vermeer S, Chapple JP: **A reduction in Drp1-mediated fission compromises mitochondrial health in autosomal recessive spastic ataxia of Charlevoix Saguenay**. *Hum Mol Genet* 2016.
10. Criscuolo C, Procaccini C, Meschini MC, Cianflone A, Carbone R, Doccini S, Devos D, Nesti C, Vuillaume I, Pellegrino M *et al*: **Powerhouse failure and oxidative damage in autosomal recessive spastic ataxia of Charlevoix-Saguenay**. *Journal of neurology* 2015, **262**(12):2755-2763.

11. Anesti V, Scorrano L: **The relationship between mitochondrial shape and function and the cytoskeleton**. *Biochim Biophys Acta* 2006, **1757**(5-6):692-699.
12. Chen H, Chan DC: **Mitochondrial dynamics--fusion, fission, movement, and mitophagy--in neurodegenerative diseases**. *HumMolGenet* 2009, **18**(R2):R169-R176.
13. Styers ML, Salazar G, Love R, Peden AA, Kowalczyk AP, Faundez V: **The endo-lysosomal sorting machinery interacts with the intermediate filament cytoskeleton**. *Mol Biol Cell* 2004, **15**(12):5369-5382.
14. Zaarur N, Meriin AB, Bejarano E, Xu X, Gabai VL, Cuervo AM, Sherman MY: **Proteasome failure promotes positioning of lysosomes around the aggresome via local block of microtubule-dependent transport**. *Mol Cell Biol* 2014, **34**(7):1336-1348.
15. Baets J, Deconinck T, Smets K, Goossens D, Van den Bergh P, Dahan K, Schmedding E, Santens P, Rasic VM, Van Damme P *et al*: **Mutations in SACS cause atypical and late-onset forms of ARSACS**. *Neurology* 2010, **75**(13):1181-1188.
16. Kumemura H, Harada M, Omary MB, Sakisaka S, Suganuma T, Namba M, Sata M: **Aggregation and loss of cytokeratin filament networks inhibit golgi organization in liver-derived epithelial cell lines**. *Cell Motil Cytoskeleton* 2004, **57**(1):37-52.
17. Perez-Olle R, Lopez-Toledano MA, Goryunov D, Cabrera-Poch N, Stefanis L, Brown K, Liem RK: **Mutations in the neurofilament light gene linked to Charcot-Marie-Tooth disease cause defects in transport**. *J Neurochem* 2005, **93**(4):861-874.
18. Kopito RR: **Aggresomes, inclusion bodies and protein aggregation**. *Trends Cell Biol* 2000, **10**(12):524-530.
19. Smith HL, Li W, Cheetham ME: **Molecular chaperones and neuronal proteostasis**. *Semin Cell Dev Biol* 2015, **40**:142-152.
20. Voisine C, Pedersen JS, Morimoto RI: **Chaperone networks: tipping the balance in protein folding diseases**. *Neurobiol Dis* 2010, **40**(1):12-20.
21. Garcia-Mata R, Bebok Z, Sorscher EJ, Sztul ES: **Characterization and dynamics of aggresome formation by a cytosolic GFP-chimera**. *J Cell Biol* 1999, **146**(6):1239-1254.
22. Wigley WC, Fabunmi RP, Lee MG, Marino CR, Muallem S, DeMartino GN, Thomas PJ: **Dynamic association of proteasomal machinery with the centrosome**. *J Cell Biol* 1999, **145**(3):481-490.
23. Perez-Sala D, Oeste CL, Martinez AE, Carrasco MJ, Garzon B, Canada FJ: **Vimentin filament organization and stress sensing depend on its single cysteine residue and zinc binding**. *Nat Commun* 2015, **6**:7287.
24. Komatsu M, Waguri S, Koike M, Sou YS, Ueno T, Hara T, Mizushima N, Iwata J, Ezaki J, Murata S *et al*: **Homeostatic levels of p62 control cytoplasmic inclusion body formation in autophagy-deficient mice**. *Cell* 2007, **131**(6):1149-1163.
25. Nezis IP, Simonsen A, Sagona AP, Finley K, Gaumer S, Contamine D, Rusten TE, Stenmark H, Brech A: **Ref(2)P, the Drosophila melanogaster homologue of mammalian**

p62, is required for the formation of protein aggregates in adult brain. *J Cell Biol* 2008, **180**(6):1065-1071.

26. Bjorkoy G, Lamark T, Brech A, Outzen H, Perander M, Overvatn A, Stenmark H, Johansen T: **p62/SQSTM1 forms protein aggregates degraded by autophagy and has a protective effect on huntingtin-induced cell death**. *J Cell Biol* 2005, **171**(4):603-614.
27. Ichimura Y, Kumanomidou T, Sou YS, Mizushima T, Ezaki J, Ueno T, Kominami E, Yamane T, Tanaka K, Komatsu M: **Structural basis for sorting mechanism of p62 in selective autophagy**. *J Biol Chem* 2008, **283**(33):22847-22857.
28. Pankiv S, Clausen TH, Lamark T, Brech A, Bruun JA, Outzen H, Overvatn A, Bjorkoy G, Johansen T: **p62/SQSTM1 binds directly to Atg8/LC3 to facilitate degradation of ubiquitinated protein aggregates by autophagy**. *J Biol Chem* 2007, **282**(33):24131-24145.
29. Gentil BJ, Minotti S, Beange M, Baloh RH, Julien JP, Durham HD: **Normal role of the low-molecular-weight neurofilament protein in mitochondrial dynamics and disruption in Charcot-Marie-Tooth disease**. *FASEB journal : official publication of the Federation of American Societies for Experimental Biology* 2012, **26**(3):1194-1203.
30. Tang HL, Lung HL, Wu KC, Le AH, Tang HM, Fung MC: **Vimentin supports mitochondrial morphology and organization**. *Biochem J* 2008, **410**(1):141-146.
31. Liu T, Guevara OE, Warburton RR, Hill NS, Gaestel M, Kayyali US: **Regulation of vimentin intermediate filaments in endothelial cells by hypoxia**. *Am J Physiol Cell Physiol* 2010, **299**(2):C363-373.
32. Hubert V, Peschel A, Langer B, Groger M, Rees A, Kain R: **LAMP-2 is required for incorporating syntaxin-17 into autophagosomes and for their fusion with lysosomes**. *Biol Open* 2016, **5**(10):1516-1529.
33. Korolchuk VI, Rubinsztein DC: **Regulation of autophagy by lysosomal positioning**. *Autophagy* 2011, **7**(8):927-928.
34. Korolchuk VI, Saiki S, Lichtenberg M, Siddiqi FH, Roberts EA, Imarisio S, Jahreiss L, Sarkar S, Futter M, Menzies FM *et al*: **Lysosomal positioning coordinates cellular nutrient responses**. *Nat Cell Biol* 2011, **13**(4):453-460.
35. Mitra S, Tsvetkov AS, Finkbeiner S: **Protein turnover and inclusion body formation**. *Autophagy* 2009, **5**(7):1037-1038.
36. Yue Z, Friedman L, Komatsu M, Tanaka K: **The cellular pathways of neuronal autophagy and their implication in neurodegenerative diseases**. *Biochim Biophys Acta* 2009, **1793**(9):1496-1507.
37. Mali P, Yang L, Esvelt KM, Aach J, Guell M, DiCarlo JE, Norville JE, Church GM: **RNA-guided human genome engineering via Cas9**. *Science* 2013, **339**(6121):823-826.
38. Yusa K, Rashid ST, Strick-Marchand H, Varela I, Liu PQ, Paschon DE, Miranda E, Ordonez A, Hannan NR, Rouhani FJ *et al*: **Targeted gene correction of alpha1-**

antitrypsin deficiency in induced pluripotent stem cells. *Nature* 2011, **478**(7369):391-394.

Figure Legends

Figure 1. Abnormal accumulations of vimentin intermediate filament in ARSACS patient HDFs.

(A) Representative confocal images of five ARSACS patient HDFs and a wild-type (WT) control HDF line (further patient and control lines are shown in Figure S2) that were stained for mitochondria (MitoTracker) and immunolabeled for vimentin. Cells were also stained with DAPI to detect nuclei. Arrows indicate areas of abnormal perinuclear vimentin accumulation. Scale bars = 10 μm. **(B)** The percentage of cells with a collapsed vimentin network was then quantified for each cell line. This was done blind to experimental status with >120 cells scored per cell line. Results are expressed as mean ± SEM for each control and patient cell line. **(C)** Representative confocal images of HDFs from a homozygous ARSACS patient with the mutation p.2801delQ and a wild-type control line. HDFs were processed for immunofluorescent detection of sacsin and vimentin, and were counterstained with DAPI for nuclei. Localisation of sacsin to the area of perinuclear vimentin accumulation is indicated by an arrow. Red dotted line indicates the edge of the cell. Scale bars = 10 μm. **(D)** Representative transmission electron micrographs (TEM) of a HDF cell from a wild-type control and ARSACS patient (p.R2002fs & p.Q4054*). Boxes delineated by white lines indicate position of zoomed images shown in panels i and ii. Red dotted line indicates the approximate boundary of the area of accumulation of filamentous material. Examples of filaments are indicated with arrows. Scale bar = 5 μm.

Figure 2. Abnormal accumulations of vimentin intermediate filament in sacsin knockdown cells. (A) Representative confocal images of wild-type HDFs cotransfected with mitoDSRed and either a non-targeting siRNA or siRNA targeting sacsin (*SACS)*. 48 hours after transfection, cells were processed for immunofluorescent detection of vimentin and counterstained with DAPI for nuclei. Scale bars = 10μm. **(B)** Representative confocal images of CRISPR generated *SACS*$^{-/-}$ HEK293 cells and *SACS*$^{-/-}$ HEK293 transfected with a plasmid for expression of full-length sacsin-GFP. Cells were processed for immunofluorescent detection of vimentin and counterstained with DAPI. **(C)** The percentage of cells with a collapsed vimentin network was then quantified for each condition. This was done blind to experimental status with >45 cells scored per condition. Results are expressed as mean ± SEM. **(D)** Sacsin immunoblot of total lysates from control and *SACS*$^{-/-}$ HEK293 cells. β-actin was used as a loading control.

Figure 3. ARSACS HDFs show characteristics of aggresome formations, including accumulation of vimentin around the MTOC and Golgi fragmentation. (A-B) Representative confocal images of two ARSACS patient HDFs lines (heterozygous mutations c.2094-2A>G/Q4054* and the homozygous mutation p.2801delQ) and a wild-type (WT) control (further patient and control lines are shown in Figure S3). Cell were stained with MitoTracker before being

processed for immunofluorescent detection of **(A)** vimentin and β-tubulin, or **(B)** GS28, a membrane protein of the cis-Golgi. Cells were counterstained with DAPI for nuclei. White boxes are shown as zoomed images in the right-hand panels. Arrows indicate areas of mitochondrial network disruption. Scale bars = 10 μm.

Figure 4. Components of the cellular proteostasis machinery localise to the vimentin cage that forms in ARSACS patient HDFs. (A-B) Representative confocal images of two ARSACS patient HDFs lines (heterozygous mutations c.2094-2A>G/p.Q4054* and the homozygous mutation p.2801delQ) and a wild-type (WT) control (further patient and control lines are shown in Figure S4). Cells were immunolabeled for **(A)** HSP70 and vimentin, or **(B)** ubiquitin and vimentin, as well as mitochondria (MitoTracker) and nuclei (DAPI). White arrows indicate perinuclear accumulation of HSP70 or ubiquitin. White boxes in merged panels are shown zoomed. Scale bars = 10 μm. **(C-D)** The incidence of cells with perinulear localisation of **(C**) HSP70 or **(D)** ubiquitin was quantified. For ubiquitin, quantification was performed in cells cultured under control conditions (vehicle only) or treated with the proteasome inhibitor MG132 for 3 hours. Results are expressed as mean ± SEM. **(E)** Immunoblot analysis of total cell lysates from five ARSACS patient and five WT control HDFs probed with an anti-HSP70 antibody. GAPDH was used as a loading control. **(F)** Densitometric analyses were performed and mean relative HSP70 protein levels calculated for the five WT and five patient cell lines. Data were normalised to GAPDH. **(G)** Immunoblot analysis of total cell lysates from five ARSACS patient and five WT control HDFs cultured for 3 hours in the presence of MG132 or vehicle only control, probed with an anti-ubiquitin antibody. GAPDH was used as a loading control.

Figure 5. Components of the autophagy-lysosome pathway localise to the vimentin cage that forms in ARSACS patient HDFs. (A-B) Representative confocal images of two ARSACS patient HDFs lines (heterozygous mutations c.2094-2A>G/p.Q4054* and the homozygous mutation p.2801delQ) and a wild-type (WT) control (further patient and control lines are shown in Figure S5). Cells were stained for mitochondria (MitoTracker) and then immunolabeled for **(A)** LAMP-2 (lysosome-associated membrane protein 2) and vimentin, or **(B**) p62/SQSTM1. Cells were also stained with DAPI to detect nuclei. White boxes in the merged panels are shown zoomed in the right-hand panels. Arrows indicate areas of LAMP-2 or p62 accumulation. Scale bars = 10 μm. **(C-D)** The incidence of cells with perinulear localisation of **(C**) Lamp2 or **(D)** p62 was quantified. **(E-F)** Immunoblot of total cell lysates from five ARSACS patient and five WT control HDFs probed with an anti-Lamp2 antibody and subsequent densitometric analyses. **(G-H)** Immunoblot of total cell lysates from five ARSACS patient and five WT control HDFs probed with an anti-p62 antibody and subsequent densitometric analyses. Data were normalised to GAPDH.

Figure 6. Autopahgic Flux is increased in ARSACS patient HDFs upon nutrient starvation.

(A) Representative EM image of autophagosomes (arrowheads) in the area of intermediate filament (arrows) accumulation in an ARSACS HDF. Scale bar = 1µm. **(B)** Representative confocal images of two ARSACS patient HDFs lines (heterozygous mutations c.2094-2A>G/p.Q4054* and the homozygous mutation p.2801delQ) and a wild-type (WT) control immunolabeled for endogenous LC3. Scale bar = 10 µm. **(C)** Quantification of the number of LC3 puncta in ARSACS and control HDF lines under basal conditions and after induction of autophagy by nutrient starvation. Puncta were quantified in 12 cells per line/treatment. Results from five control and five patient cell lines were combined to give an overall mean ± SEM, $^{***}p<0.001$. **(D)** Immunoblot analysis of total cell lysates from ARSACS patient and WT control HDFs probed with an LC3 antibody to detect LC3-I and LC3-II. Cell lysates were collected from untreated cells, nutrient starved cells, and cells that were nutrient starved and treated with either bafilomycin A or 3-Methyladenine (3-MA). Actin was used as a loading control. **(E)** Densitometric analyses were performed and mean LC3-I and LC3-II levels relative to actin were calculated for each treatment in control and ARSACS HDFs (n= 4).

Figure 7. Primary neurons from the *Sacs*$^{-/-}$ mouse have abnormal neurofilament organisation, altered cellular architecture and abnormal ubiquitin localisation. (A) Representative maximum intensity projections of confocal Z-stacks of primary neurons from 4 week old dorsal root ganglia and spinal cord culture. Motor (MN) and sensory neurons (SN) from *Sacs*$^{-/-}$ (Sacs KO) or wild-type (WT) mice were immunolabeled for NFH. Arrows indicate bundled NFH intermediate filaments. **(B)** Nuclear positioning in DRG sensory neurons revealed by DAPI (blue) staining for the nucleus and immunostaining for tubulin (red) to identify the soma in the *Sacs*$^{-/-}$ sensory neuron. **(C)** Quantification of the percentage of sensory neuron with eccentric nuclear localisation. Eccentric localisation of nucleus was determined by the ratio of r1:r2, where r1 is the longest and r2 is the shortest distance between the nuclear membrane and the closest plasma membrane. Cells where r1/r2 was ≥1.1 (≥10% deviation from a centrally positioned nucleus) were scored as having an eccentric nuclear localisation **(D)** Representative confocal images of motor (MN) and sensory neurons (SN) from *Sacs*$^{-/-}$ (Sacs KO) or wild-type (WT) mice were immunolabeled for Tom20. Arrows indicate areas where mitochondria were absent. **(E)** Representative confocal images of motor neurons from *Sacs*$^{-/-}$ (Sacs KO) or wild-type (WT) mice immunolabeled for ubiquitin. **(F)** Quantification of the number of motor neurons (MN) showing a perinuclear localisation of ubiquitin. **(G)** Representative confocal images of sensory neurons from *Sacs*$^{-/-}$ (Sacs KO) or wild-type (WT) mice immunolabeled for ubiquitin. **(H)** Quantification of the number of sensory neurons (SN) showing a perinuclear localisation of ubiquitin. Arrows show areas of ubiquitin accumulation. A white asterisk indicates the location of a glial cell. Scale bars =10µm. Error bars are ± SD, $^{*}p<0.05$. N= between 30 and 70 neurons per experiment.

A

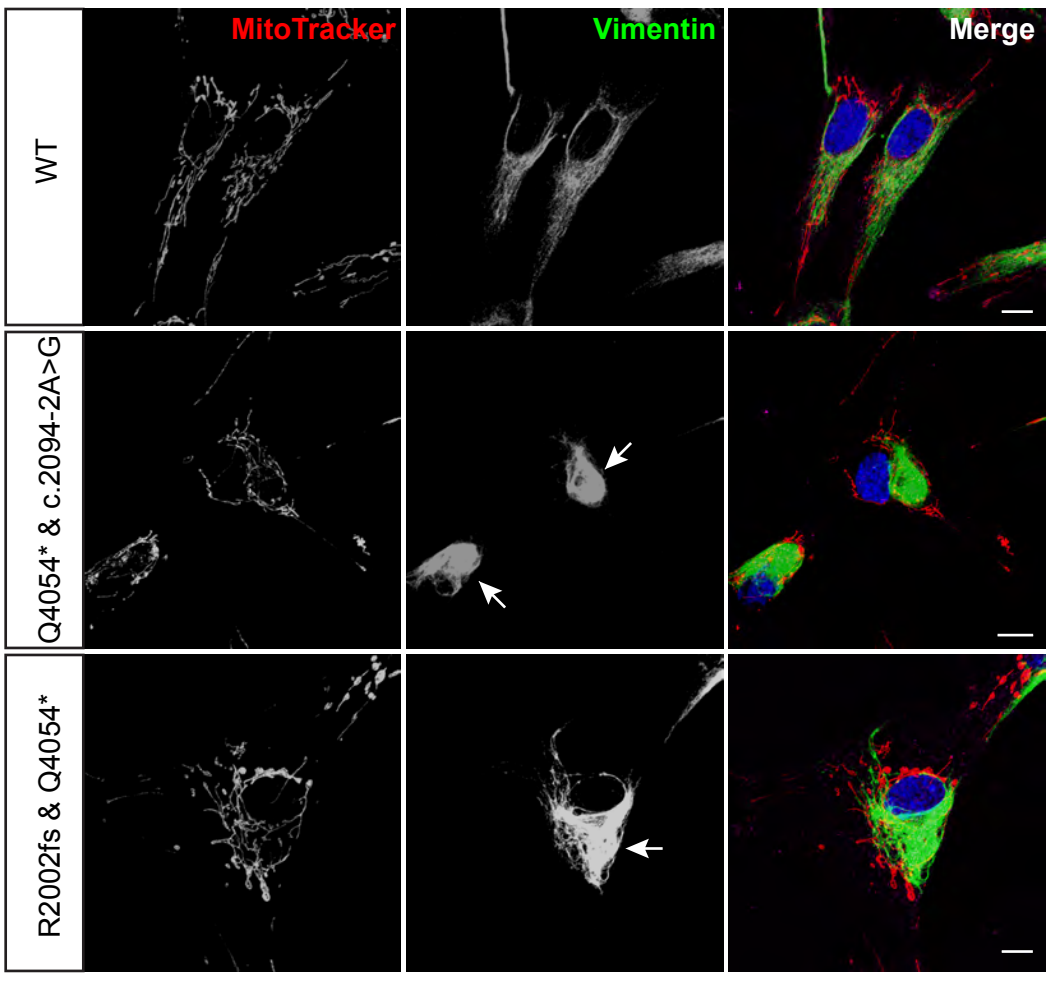
MitoTracker
Vimentin
Merge
WT
Q4054* & c.2094-2A>G
R2002fs & Q4054*

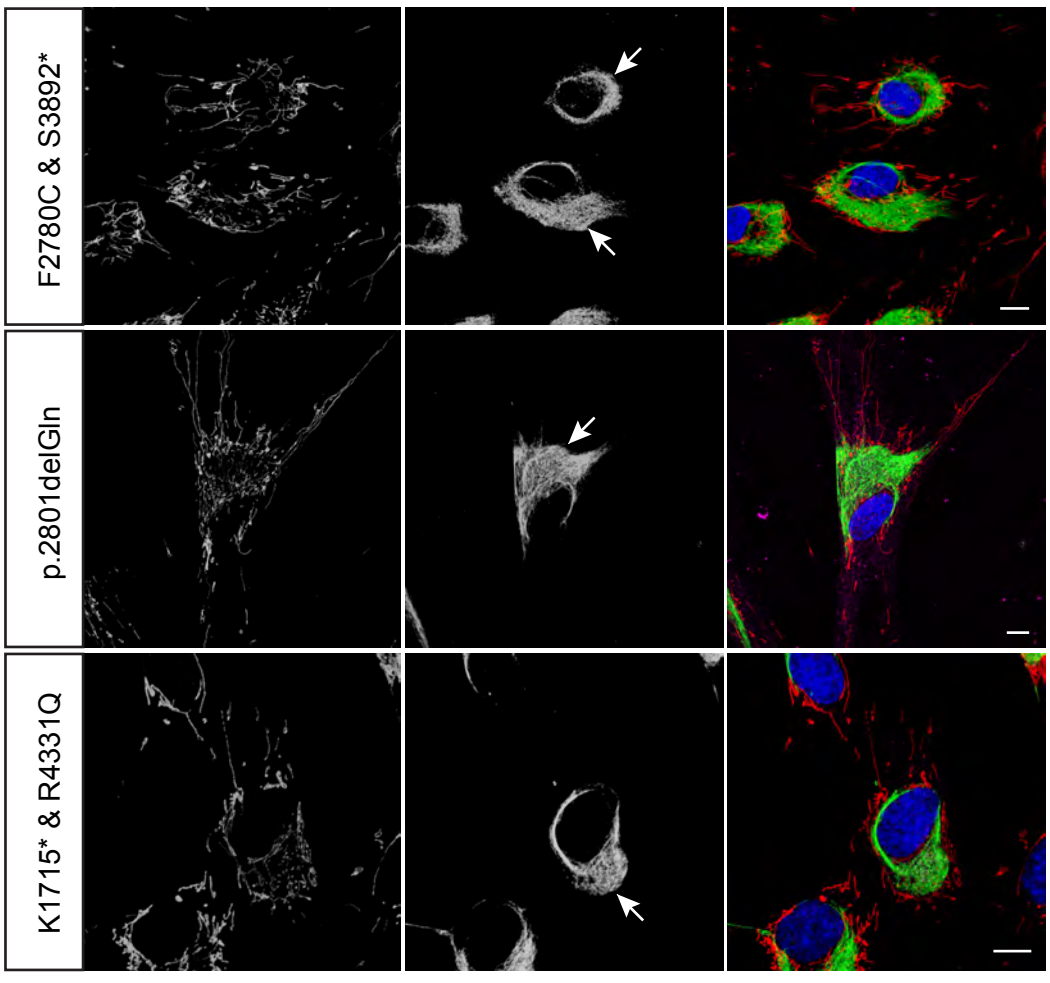
F2780C & S3892*
p.2801delGln
K1715* & R4331Q

B

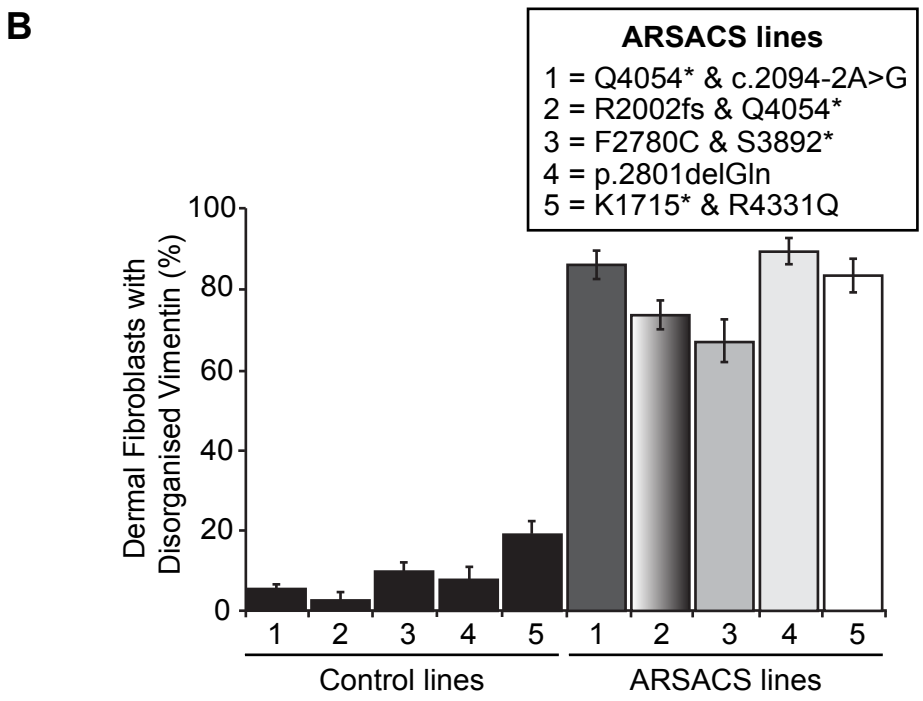
ARSACS lines
1 = Q4054* & c.2094-2A>G
2 = R2002fs & Q4054*
3 = F2780C & S3892*
4 = p.2801delGln
5 = K1715* & R4331Q
Dermal Fibroblasts with Disorganised Vimentin (%)
100
80
60
40
20
0
1 2 3 4 5 1 2 3 4 5
Control lines
ARSACS lines

C

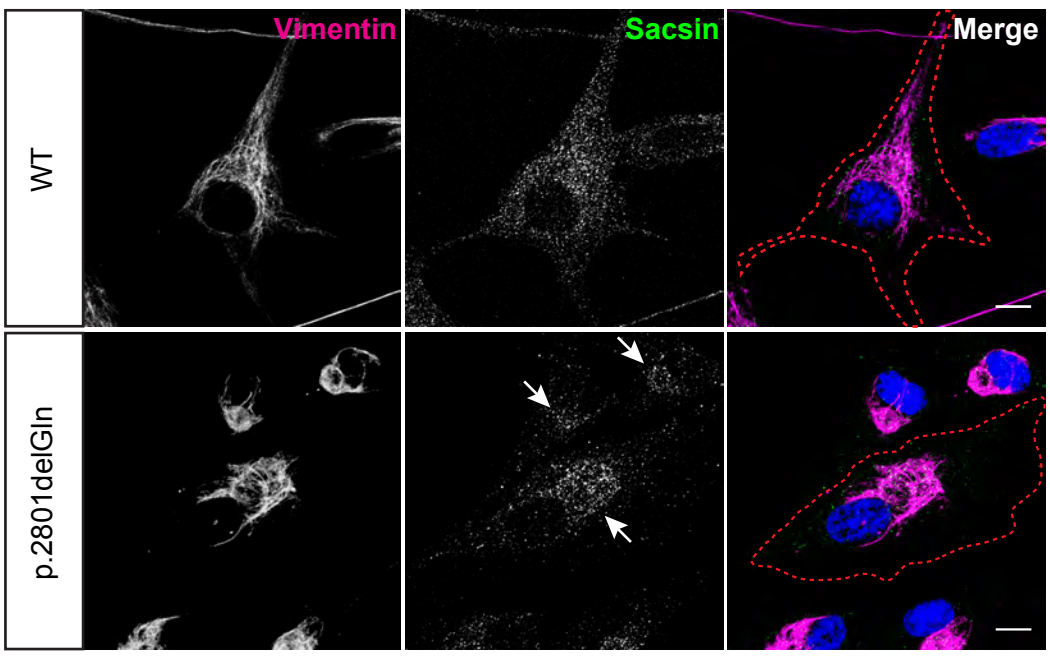
Vimentin
Sacsin
Merge
WT
p.2801delGln

D

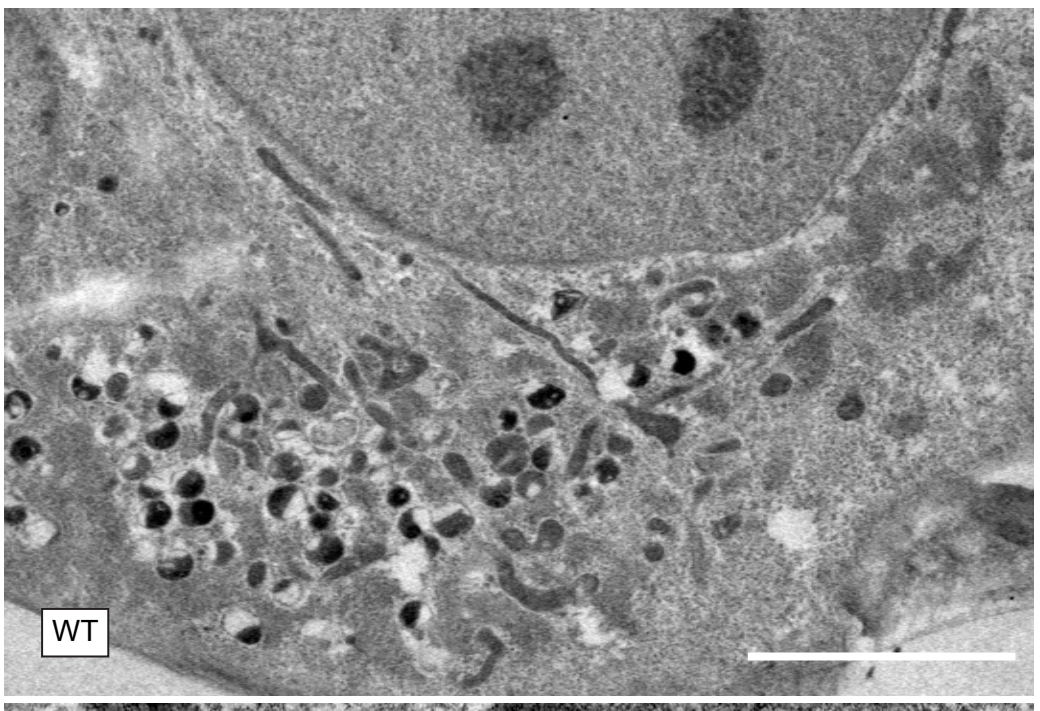
WT

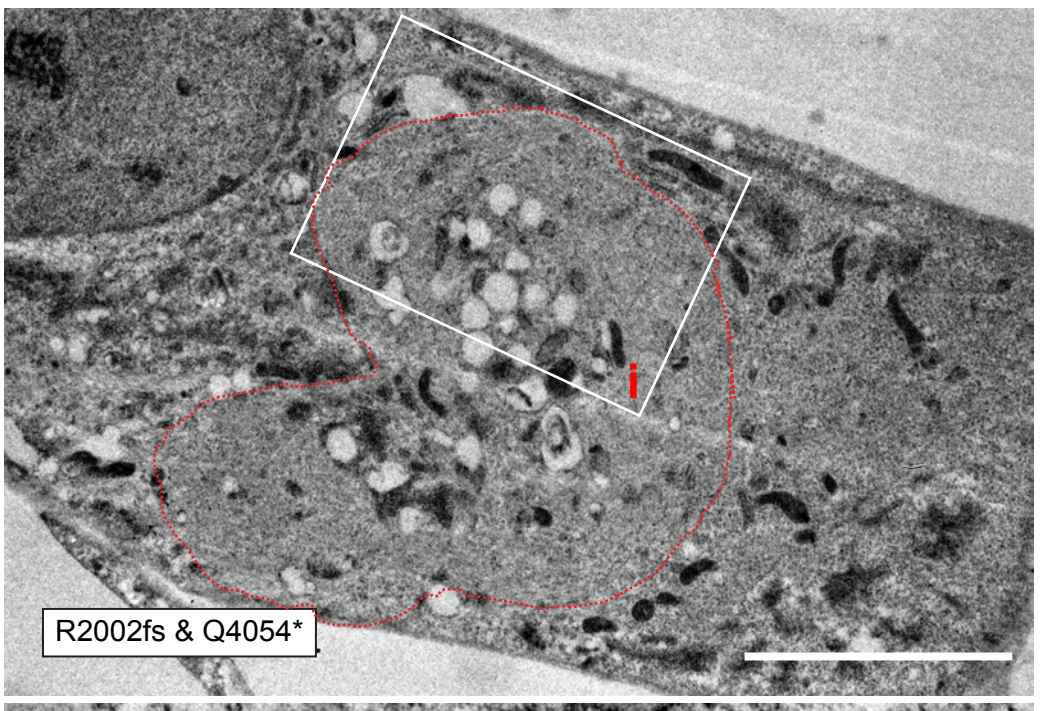
i
R2002fs & Q4054*

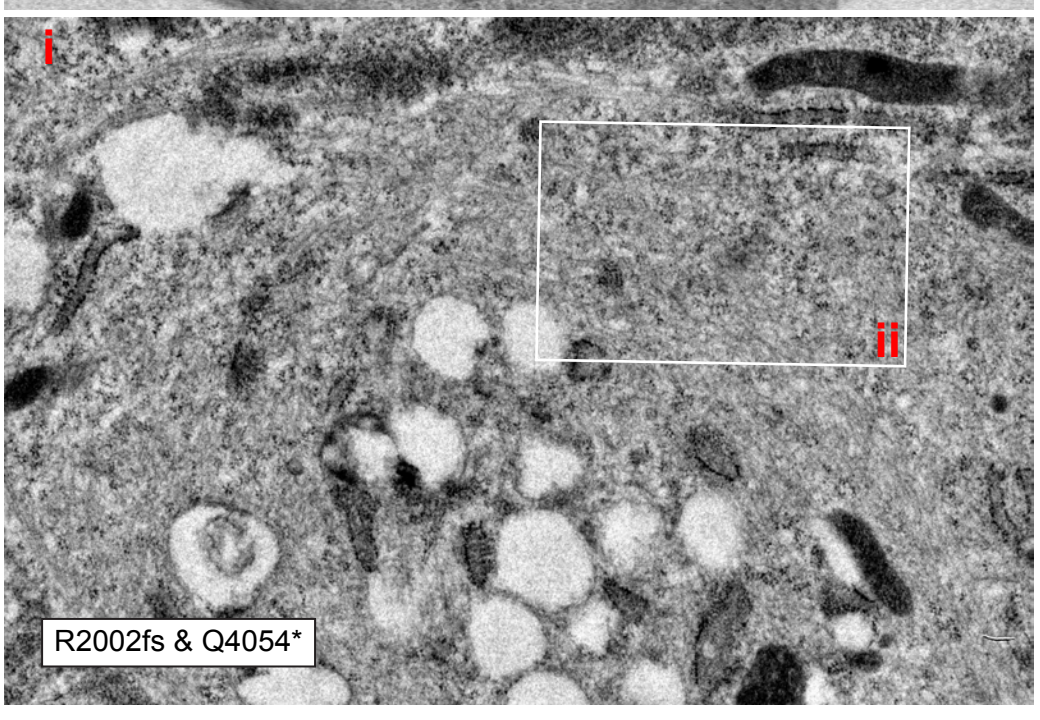
i
ii
R2002fs & Q4054*

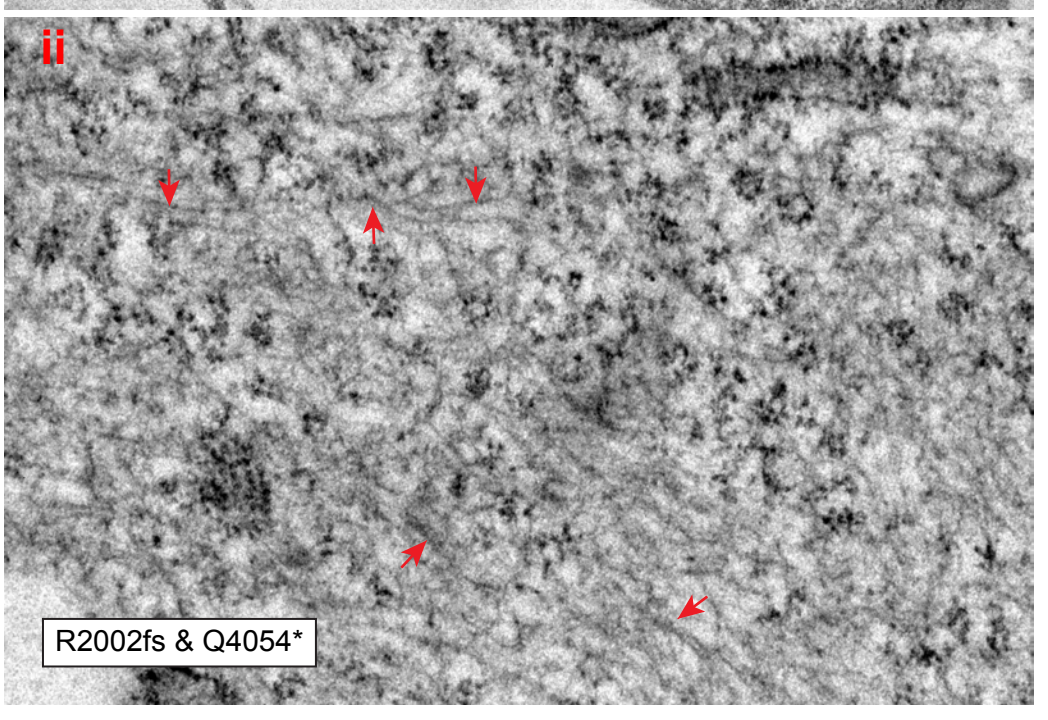
ii
R2002fs & Q4054*

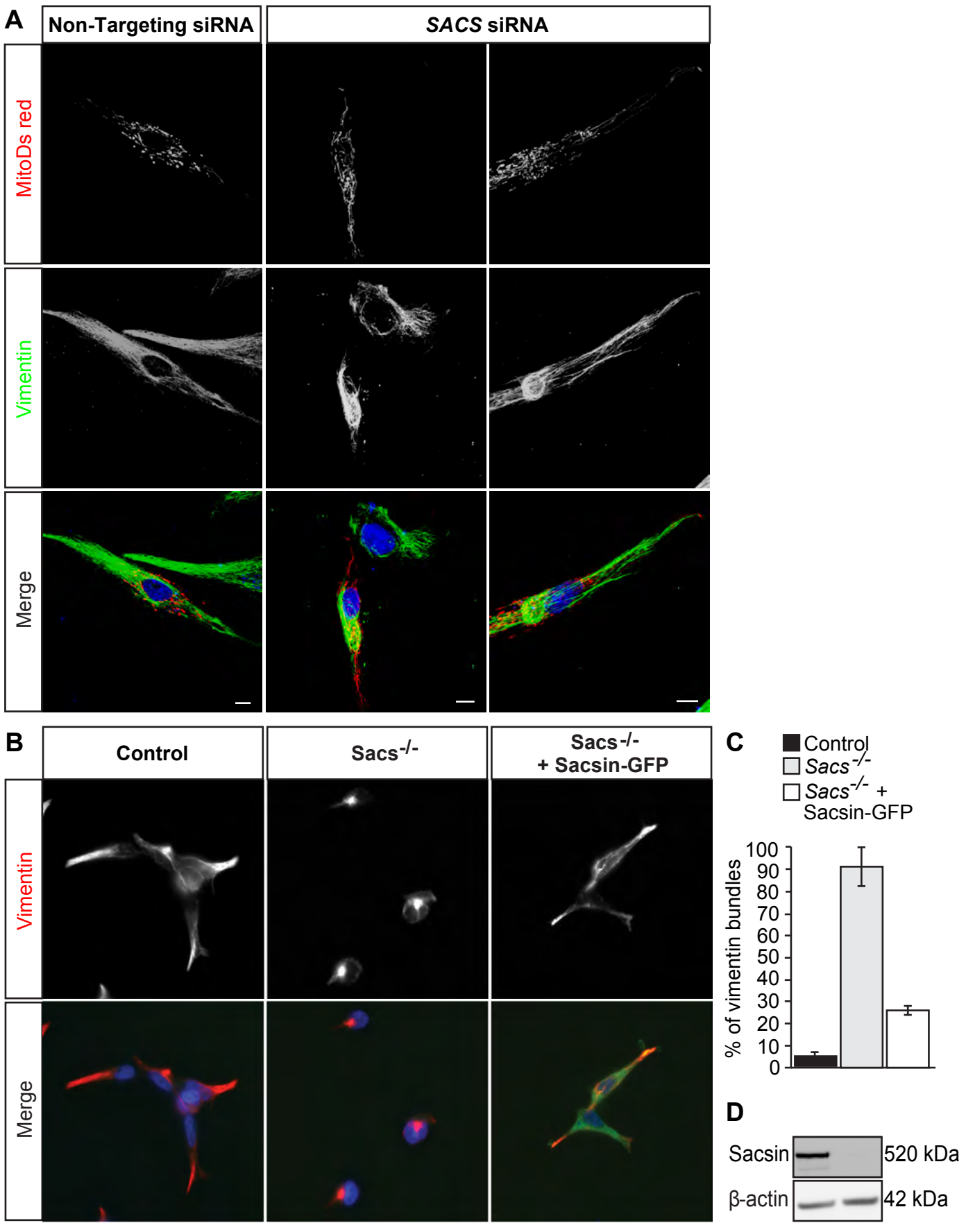
A
Non-Targeting siRNA
SACS siRNA
MitoDs red
Vimentin
Merge
B
Control
Sacs-/-
Sacs-/-
+ Sacsin-GFP
Vimentin
Merge
C
Control
Sacs-/-
Sacs-/- +
Sacsin-GFP
% of vimentin bundles
100
90
80
70
60
50
40
30
20
10
0
D
Sacsin
520 kDa
β-actin
42 kDa

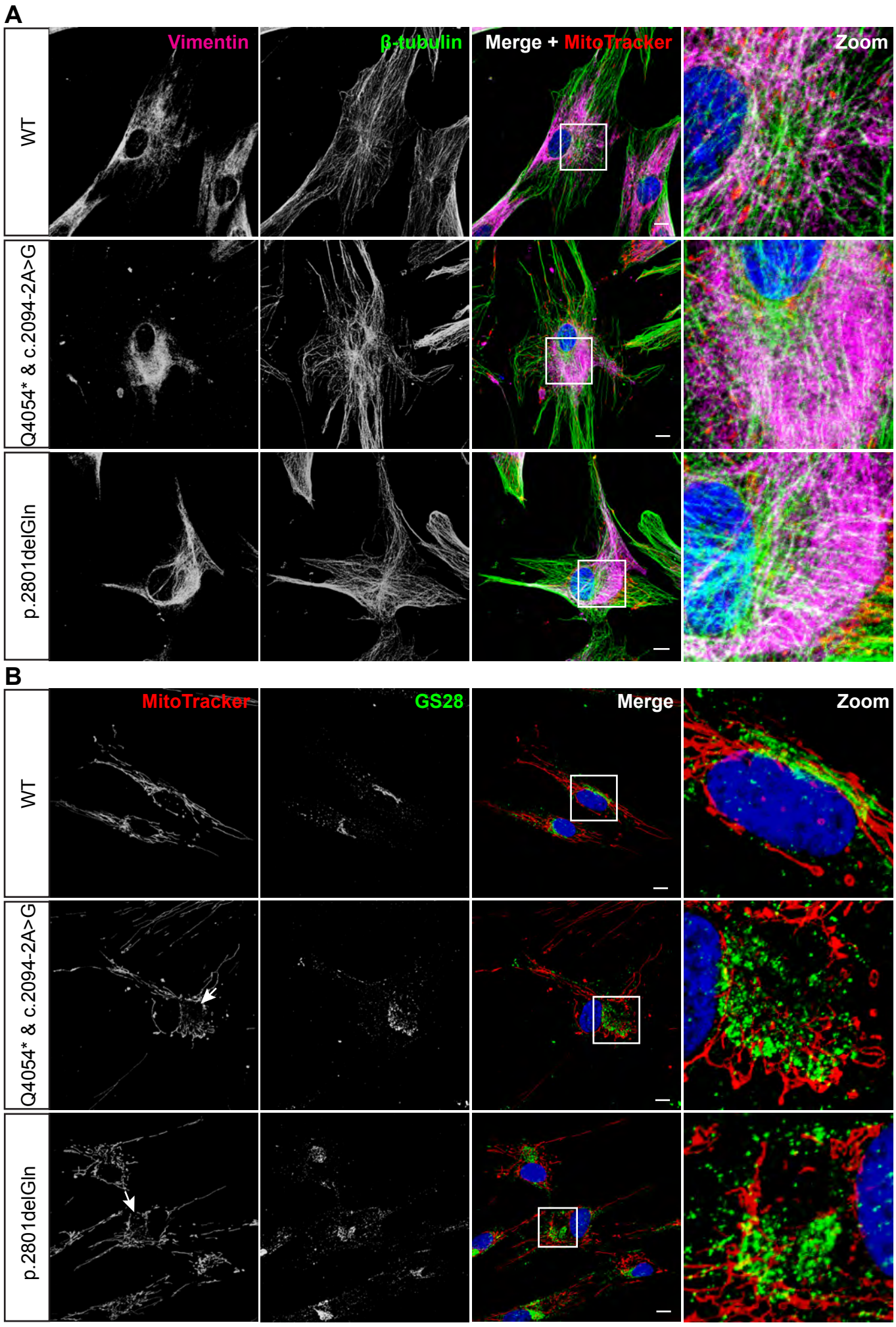
A
WT
Q4054* & c.2094-2A>G
p.2801delGln
Vimentin
β-tubulin
Merge + MitoTracker
Zoom
B
MitoTracker
GS28
Merge
Zoom

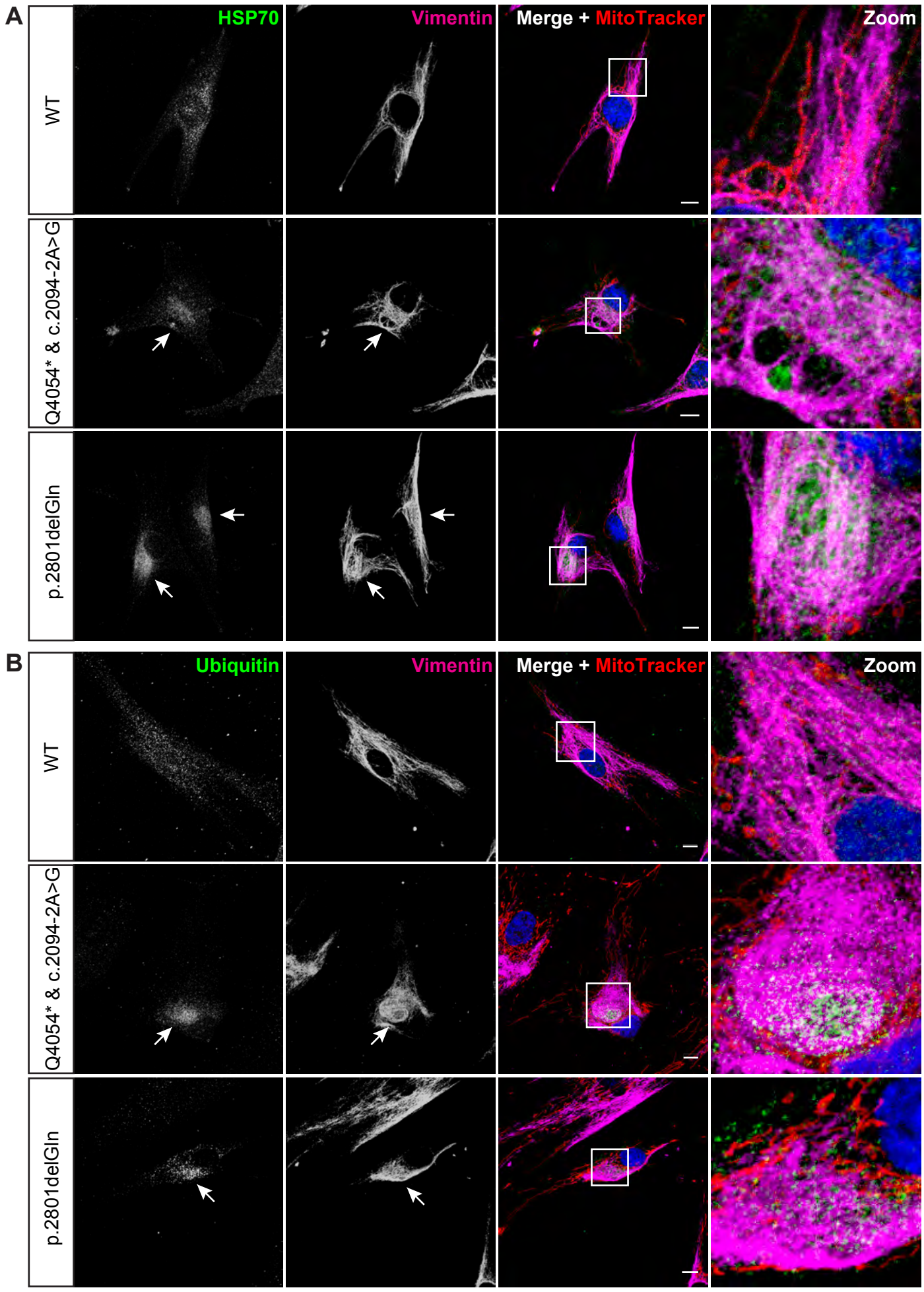
A
HSP70
Vimentin
Merge + MitoTracker
Zoom
WT
Q4054* & c.2094-2A>G
p.2801delGln
B
Ubiquitin
Vimentin
Merge + MitoTracker
Zoom
WT
Q4054* & c.2094-2A>G
p.2801delGln
C
% cells wtih HSP70 Punctae
100
80
60
40
20
0
**
Diffuse
Perinuclear
WT ARSACS
D
% cells with Ubiquitin Punctae
100
80
60
40
20
0
Diffuse
Perinuclear
- + - + MG132
WT ARSACS
E
WT
ARSACS
HSP70
GAPDH
F
Relative HSP70 protein levels
1.4
1.2
1.0
0.8
0.6
0.4
0.2
0
WT
ARSACS
G
Basal
MG132
WT
ARSACS
WT
ARSACS
260 kDa
160 kDa
10 kDa
80 kDa
160 kDa
Ubiquitin
GAPDH

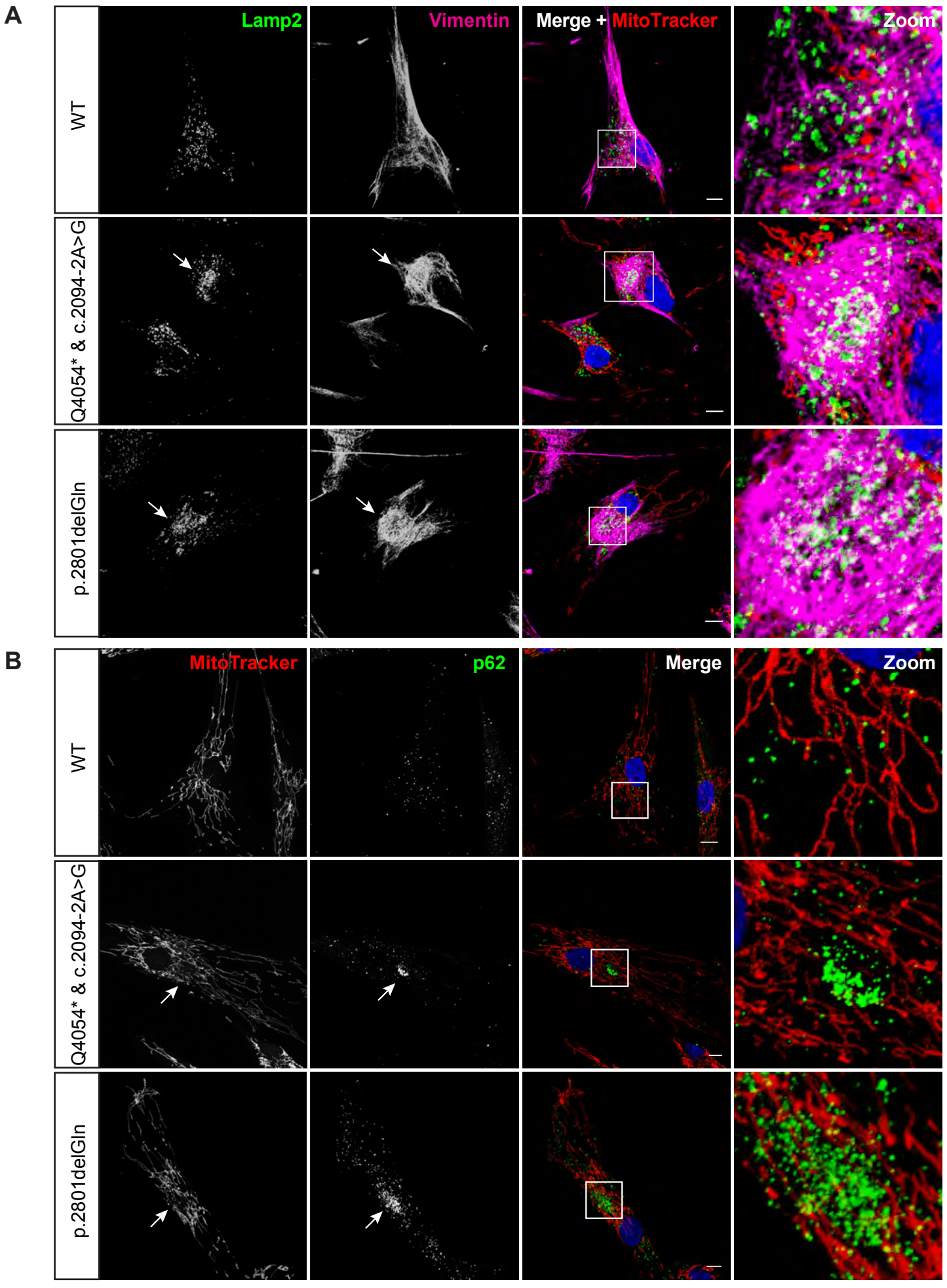
A
Lamp2
Vimentin
Merge + MitoTracker
Zoom
WT
Q4054* & c.2094-2A>G
p.2801delGln
B
MitoTracker
p62
Merge
Zoom
WT
Q4054* & c.2094-2A>G
p.2801delGln
C
Diffuse
Perinuclear
% cells with Lamp2 punctae
100
80
60
40
20
0
**
WT ARSACS
D
% cells with p62 punctae
100
80
60
40
20
0
WT ARSACS
E
WT
ARSACS
Lamp2
GAPDH
F
Relative Lamp2 protein levels
1.4
1.2
1.0
0.8
0.6
0.4
0.2
0
*
WT ARSACS
G
WT
ARSACS
p62
GAPDH
H
Relative p62 protein levels
1.2
1.0
0.8
0.6
0.4
0.2
0
*
WT ARSACS

A

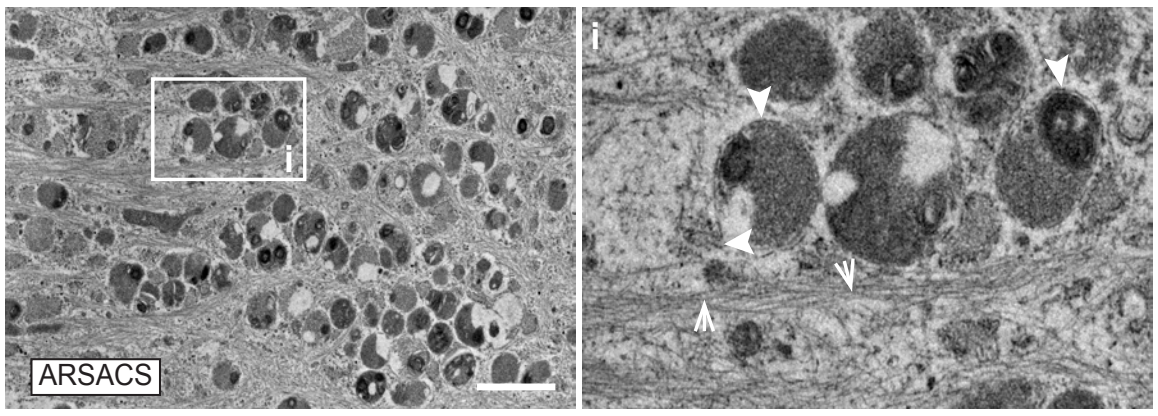
i
ARSACS
i

B

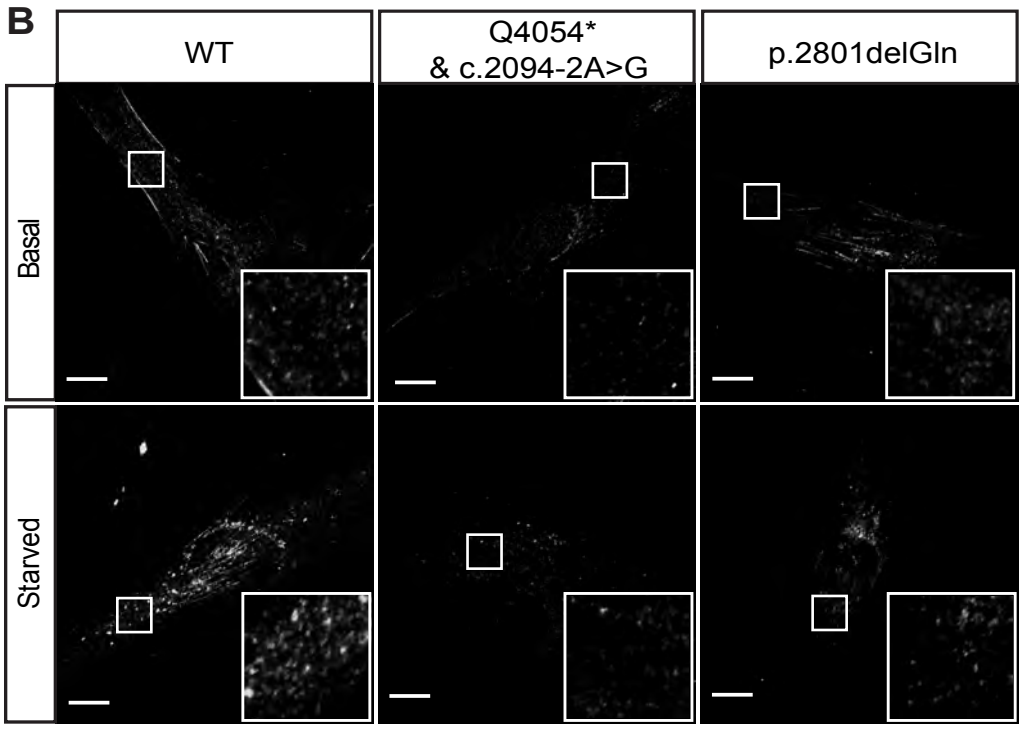
WT
Q4054*
& c.2094-2A>G
p.2801delGln
Basal
Starved

C

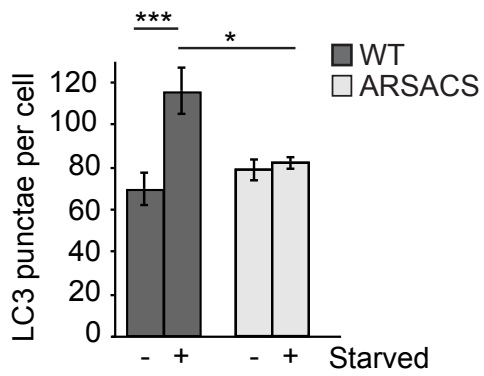
***
*
WT
ARSACS
LC3 punctae per cell
120
100
80
60
40
20
0
- + - +
Starved

D

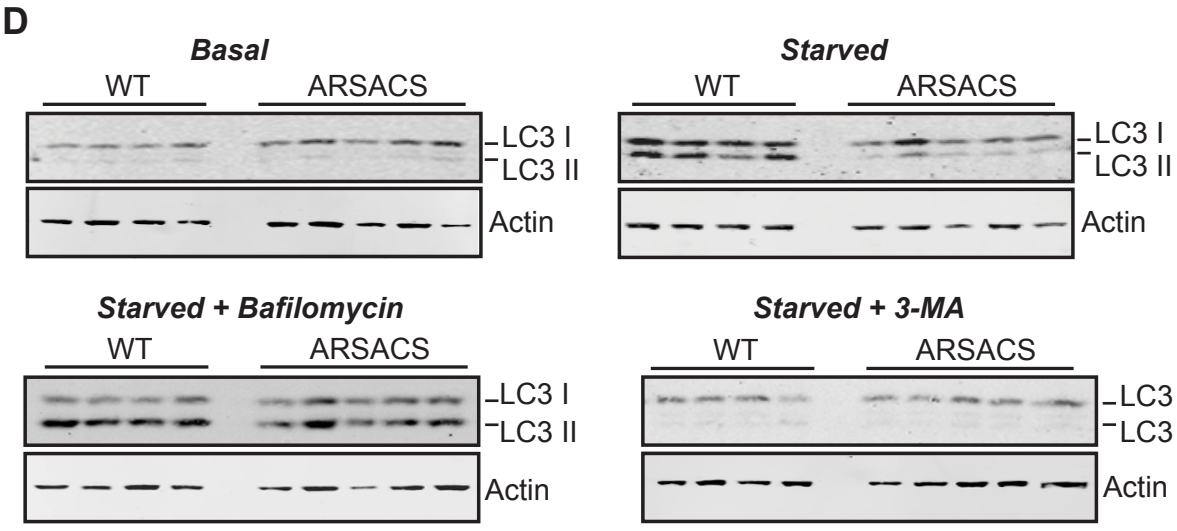
Basal
WT
ARSACS
LC3 I
LC3 II
Actin
Starved
WT
ARSACS
LC3 I
LC3 II
Actin
Starved + Bafilomycin
WT
ARSACS
LC3 I
LC3 II
Actin
Starved + 3-MA
WT
ARSACS
LC3 I
LC3 II
Actin

E

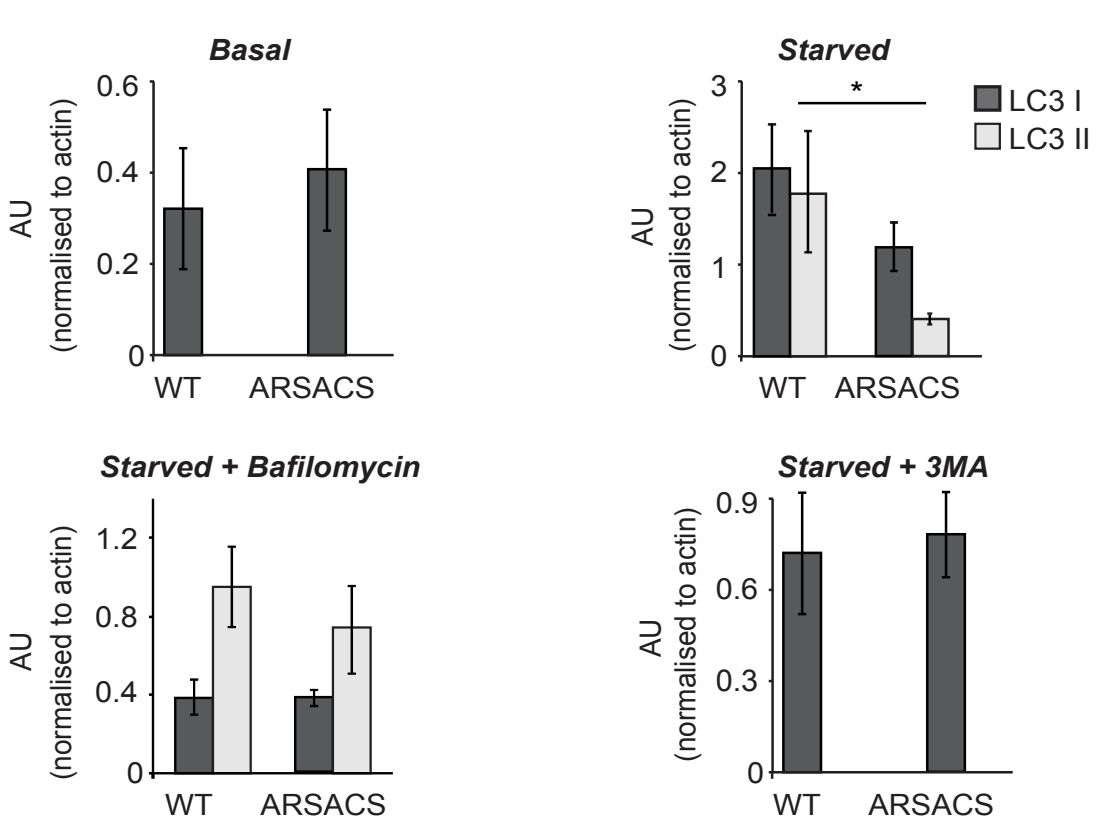
Basal
AU
(normalised to actin)
0.6
0.4
0.2
0
WT
ARSACS
Starved
AU
(normalised to actin)
3
2
1
0
*
LC3 I
LC3 II
WT
ARSACS
Starved + Bafilomycin
AU
(normalised to actin)
1.2
0.8
0.4
0
WT
ARSACS
Starved + 3MA
AU
(normalised to actin)
0.9
0.6
0.3
0
WT
ARSACS

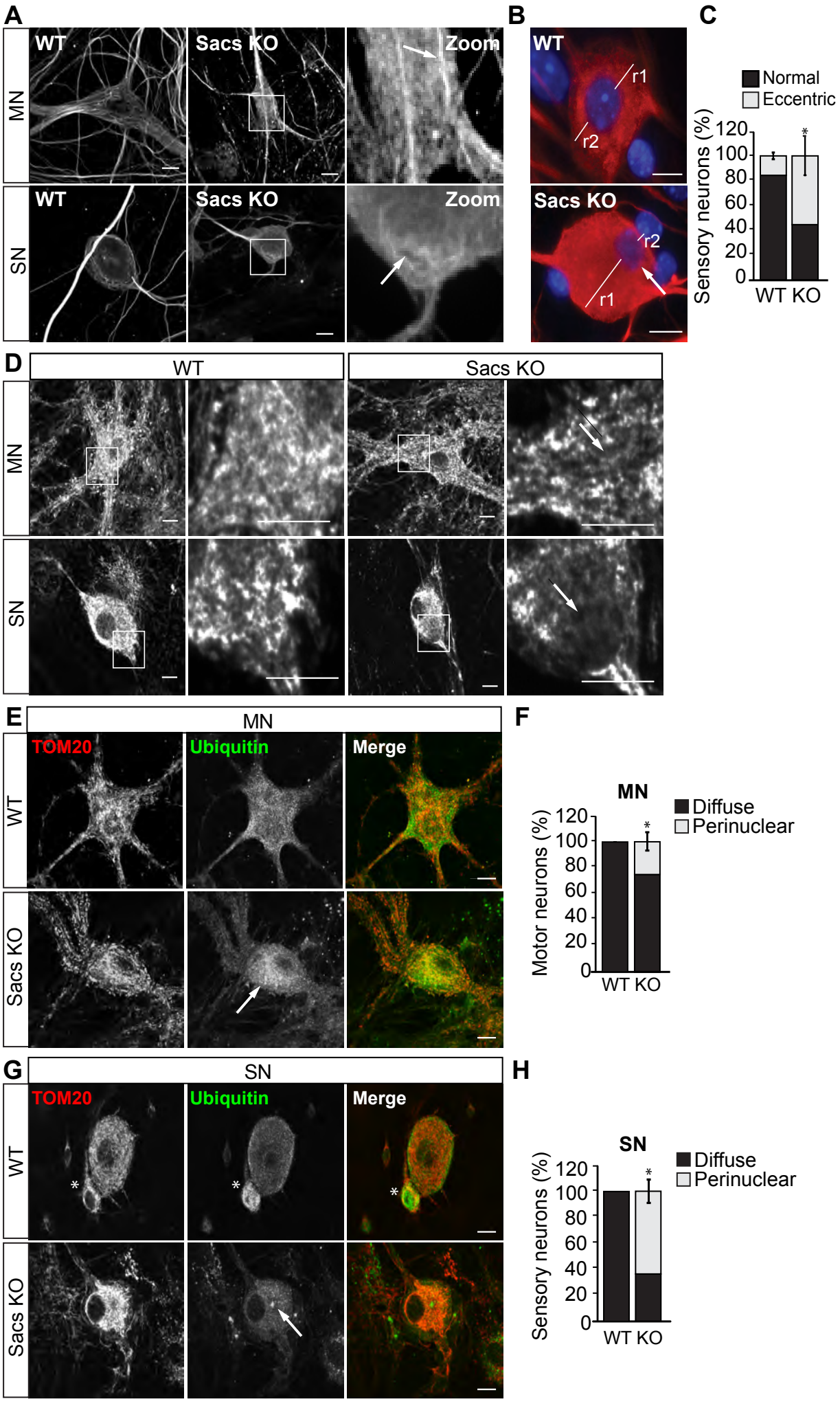
A
MN
SN
WT
Sacs KO
Zoom
B
WT
Sacs KO
r1
r2
C
Normal
Eccentric
Sensory neurons (%)
120
100
80
60
40
20
0
WT KO
*
D
WT
Sacs KO
MN
SN
E
MN
TOM20
Ubiquitin
Merge
WT
Sacs KO
F
MN
Diffuse
Perinuclear
Motor neurons (%)
120
100
80
60
40
20
0
WT KO
*
G
SN
TOM20
Ubiquitin
Merge
WT
Sacs KO
*
H
SN
Diffuse
Perinuclear
Sensory neurons (%)
120
100
80
60
40
20
0
WT KO
*

A

ARSACS patient *SACS* mutations[#]	Type of mutation	Sacsin detected by immunoblot
p.Q4054*& c.2094-2A>G	Nonsense/Splice-site	No
p.R2002fs & p.Q4054*	Frameshift/Nonsense	No
p.F2780C & p.S3892*	Missense/Nonsense	No
p.2801delQ	In frame deletion	Yes
p.K1715* & p.R4331Q	Nonsense/Missense	?
p.R3636Q : p.P3652T & p.L3745Rfs	Missense/Frameshift	No
p.R3636Q : p.P3652T & p.C72Cfs	Missense/Frameshift	Yes
c.8844delT	Nonsense	No

SACS Accession number NP_055178

[#] Top five listed cell lines were predominantly used in this study

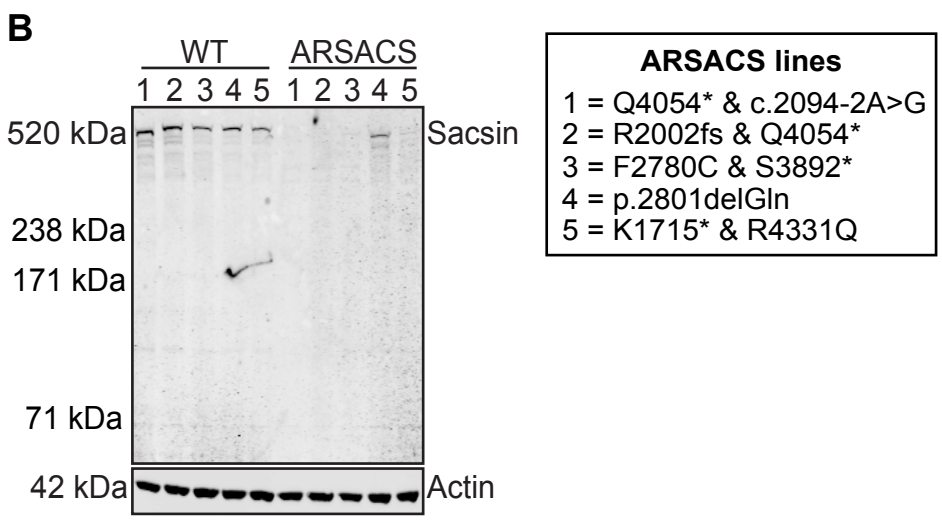

Figure S1. ARSACS HDF lines used in this study. (A) Table detailing the disease associated mutations present in sacsin for each ARSACS patient cell line used in this study. Amino acid change to an * indicates a truncated protein, fs indicates a frameshift and del indicates a deletion. For the column 'sacsin detection by immunoblot' it should be noted that the anti-sacsin antibody available recognises an epitope between amino acids 4100-4200 of sacsin. **(B)** Immunoblot to detect sacsin in total cell lysates from wild-type control and ARSACS HDFs with the mutations p.Q4054*/c.2094-2A>G, p.R2002fs/p.Q4054*, p.F2780C/p.S3892*, p.2801delGln, and p.K1715*/p.R4331Q. β-actin was used as a loading control. **(C-D)** Immunoblot to detect sacsin in cell lysates in additional ARSACS HDFs with the mutations p.R3636Q/p.P3652T/p.L3745Rfs, R3636Q/P3652T/C72Cfs, and c.8844delT.

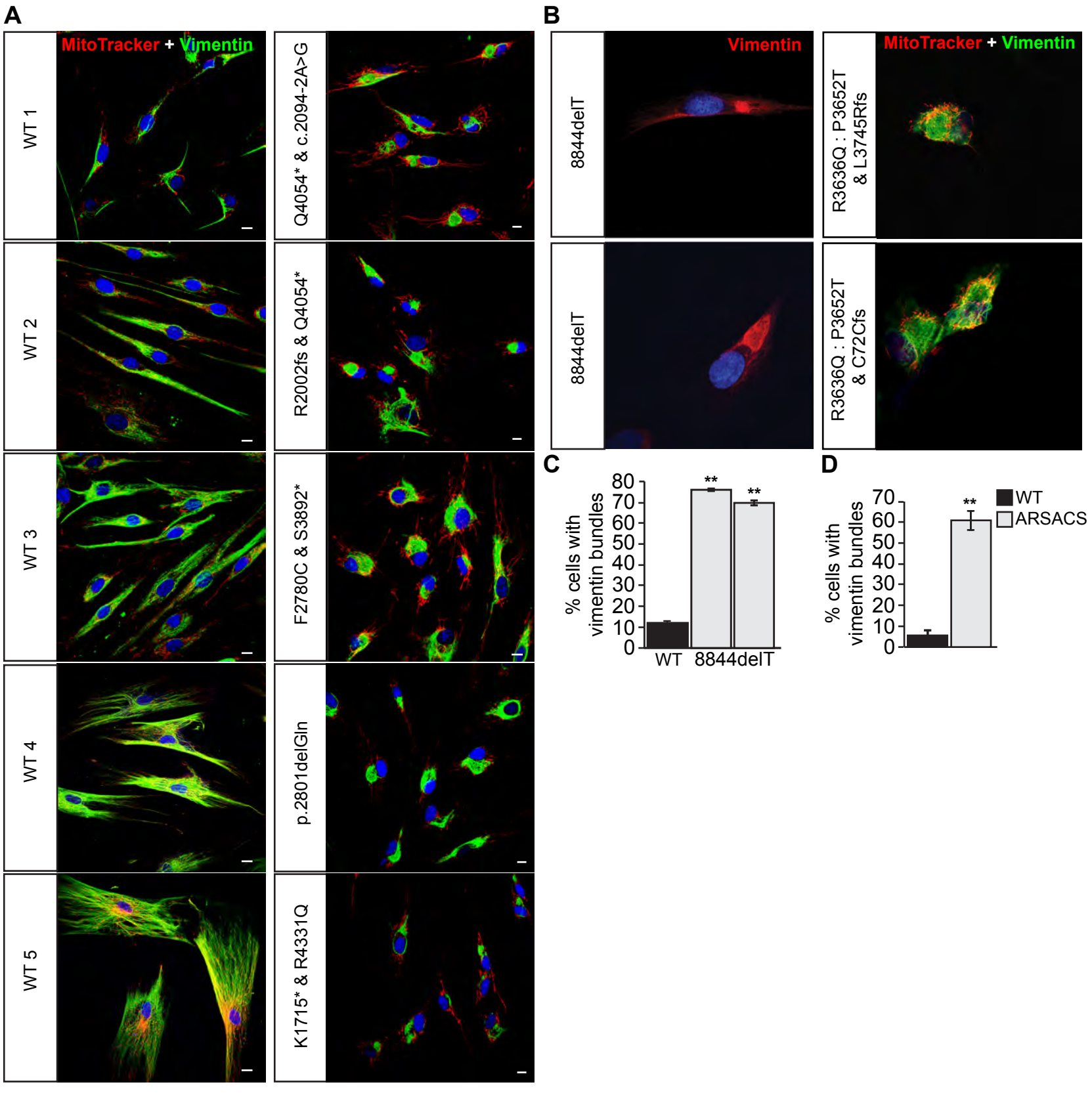

Figure S2. Abnormal accumulations of vimentin intermediate filament are present in HDFs from ARSACS patients with a range of different mutations. (A) Representative confocal images of five ARSACS patient HDFs and five wild-type (WT) control HDF lines that were stained for mitochondria (MitoTracker) and immunolabeled for vimentin. Cells were also stained with DAPI to detect nuclei. Scale bars = 10 μm. **(B)** Analyses of vimentin localisation in additional ARSACS HDFs with the mutations c.8844delT, p.R3636Q/p.P3652T/p.L3745Rfs, and p.R3636Q/p.P3652T/p.C72Cfs. **(C)** The percentage of cells with a collapsed vimentin network was quantified in the two patient cell lines that are homozygous for the c.8844delT mutation. This was done blind to experimental status with >120 cells scored per cell line. Results are expressed as mean ± SEM for wild-type and patient cell lines. **(D)** The percentage of cells with a collapsed vimentin network was quantified in the ARSACS HDFs with the mutations p.R3636Q/p.P3652T/p.L3745Rfs and p.R3636Q/p.P3652T/p.C72Cfs. This was done blind to experimental status with >120 cells scored per cell line. Results are expressed as mean ± SEM for wild-type and patient cell lines. **p<0.01.

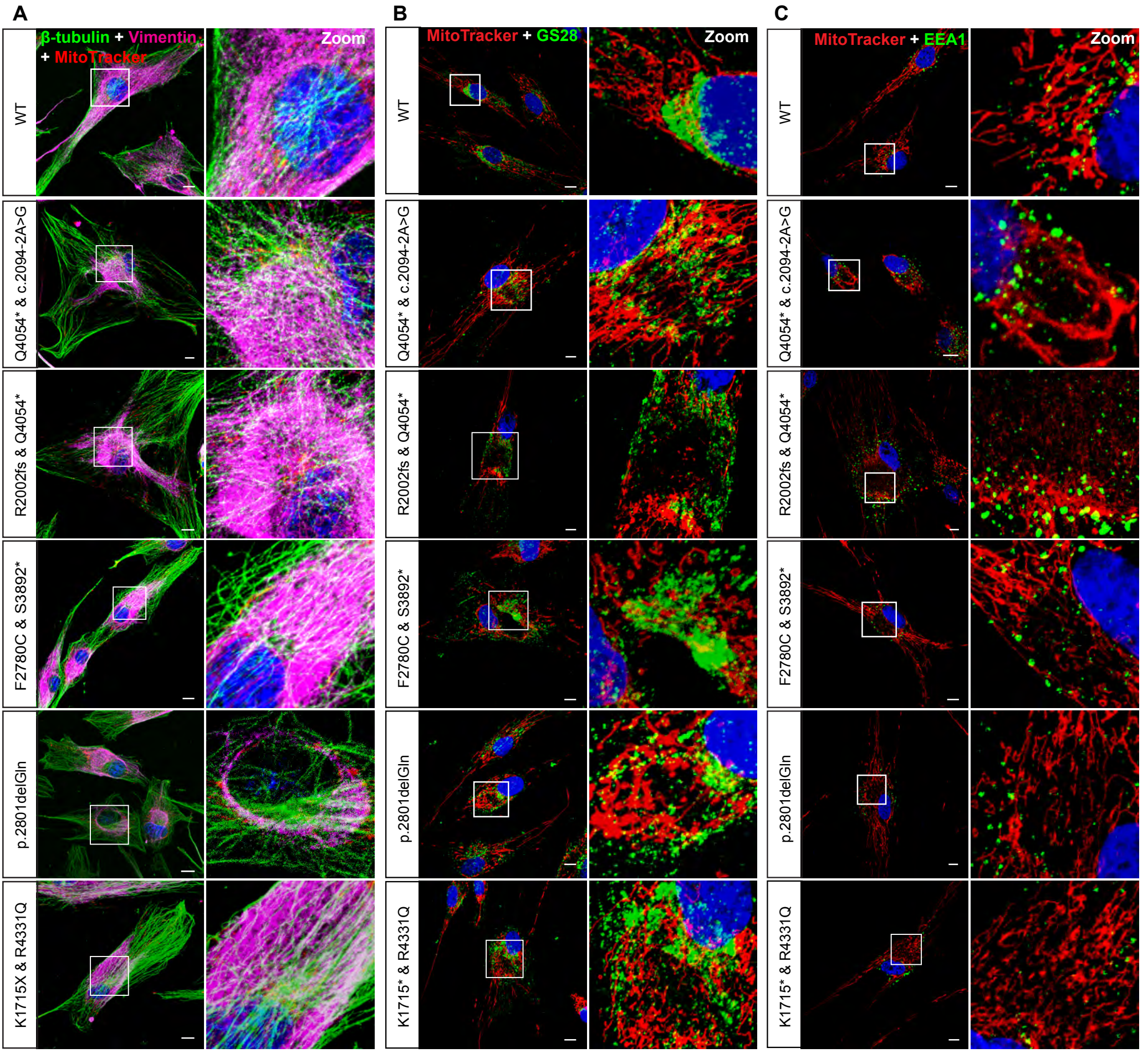

Figure S3. ARSACS patient HDFs have accumulations of vimentin in the region of the MTOC as well as altered localisation of the Golgi apparatus and early endosomes. (A-C) Representative confocal images of five ARSACS patient HDFs lines and a wild-type (WT) control. Cell were stained with MitoTracker before being processed for immunofluorescent detection of (A) β-tubulin and vimentin, **(B)** GS28 membrane protein of the cis-Golgi, or **(C)** EEA1, membrane-associated protein to early endosomes. Cells were counterstained with DAPI for nuclei. White boxes are shown as zoomed images in the right-hand panels. Scale bars = 10μm.

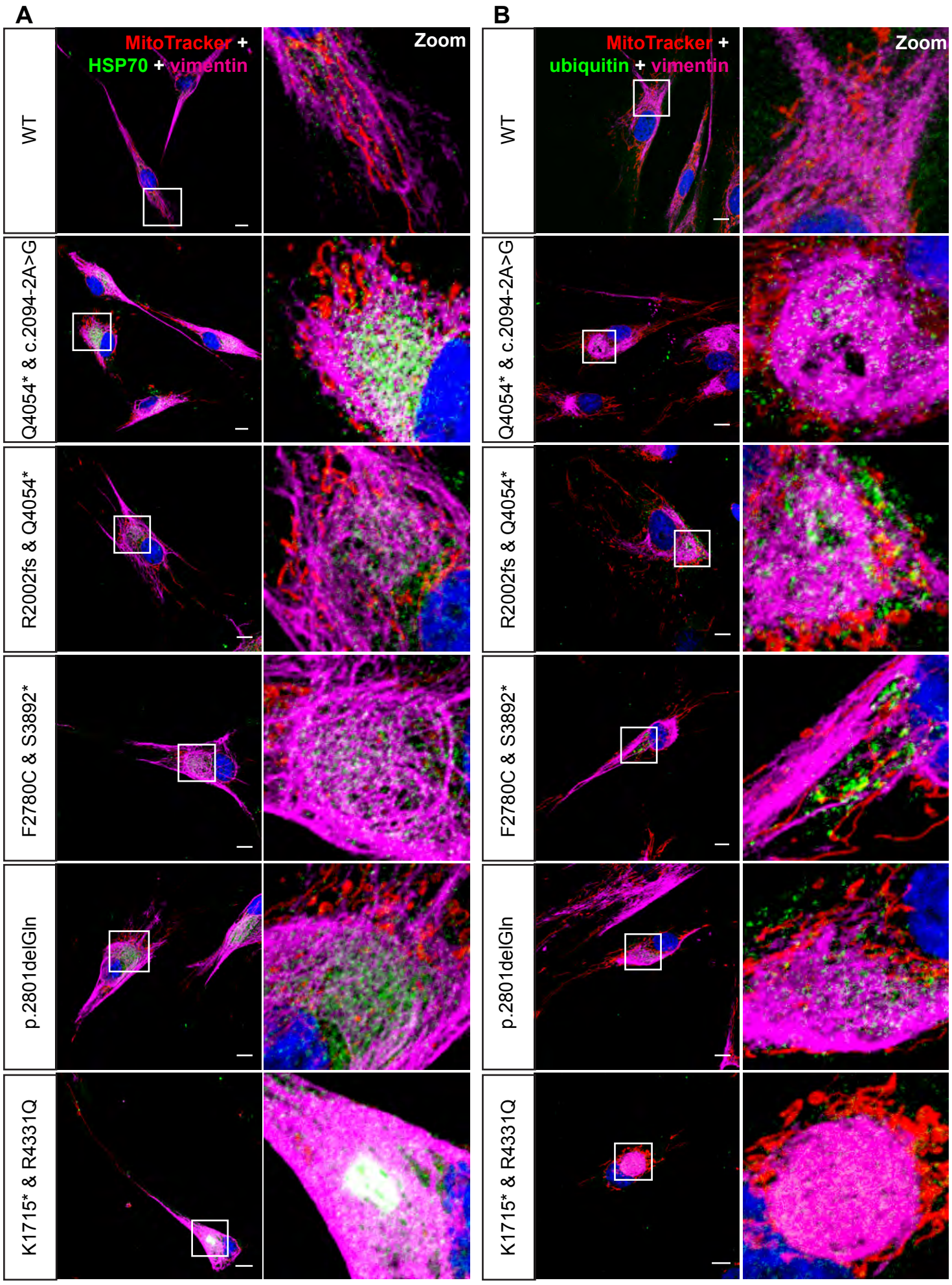

Figure S4. ARSACS patient HDFs localise components of the cellular proteostasis machinery to a vimentin cage structure. (A, B) Representative confocal images of dermal fibroblasts from ARSACS patient or wild-type (WT) control. Cells were stained with 100μM MitoTracker for 30 minutes prior to fixation and permeabilisation. Cells were incubated with antibodies to **(A)** HSP70 and vimentin, or **(B)** ubiquitin and vimentin. Confocal analysis showed accumulation of HSP70 and ubiquitin in perinuclear regions in all ARSACS patient cells. White boxes in merged panels are shown zoomed. Scale bars = 10 μm.

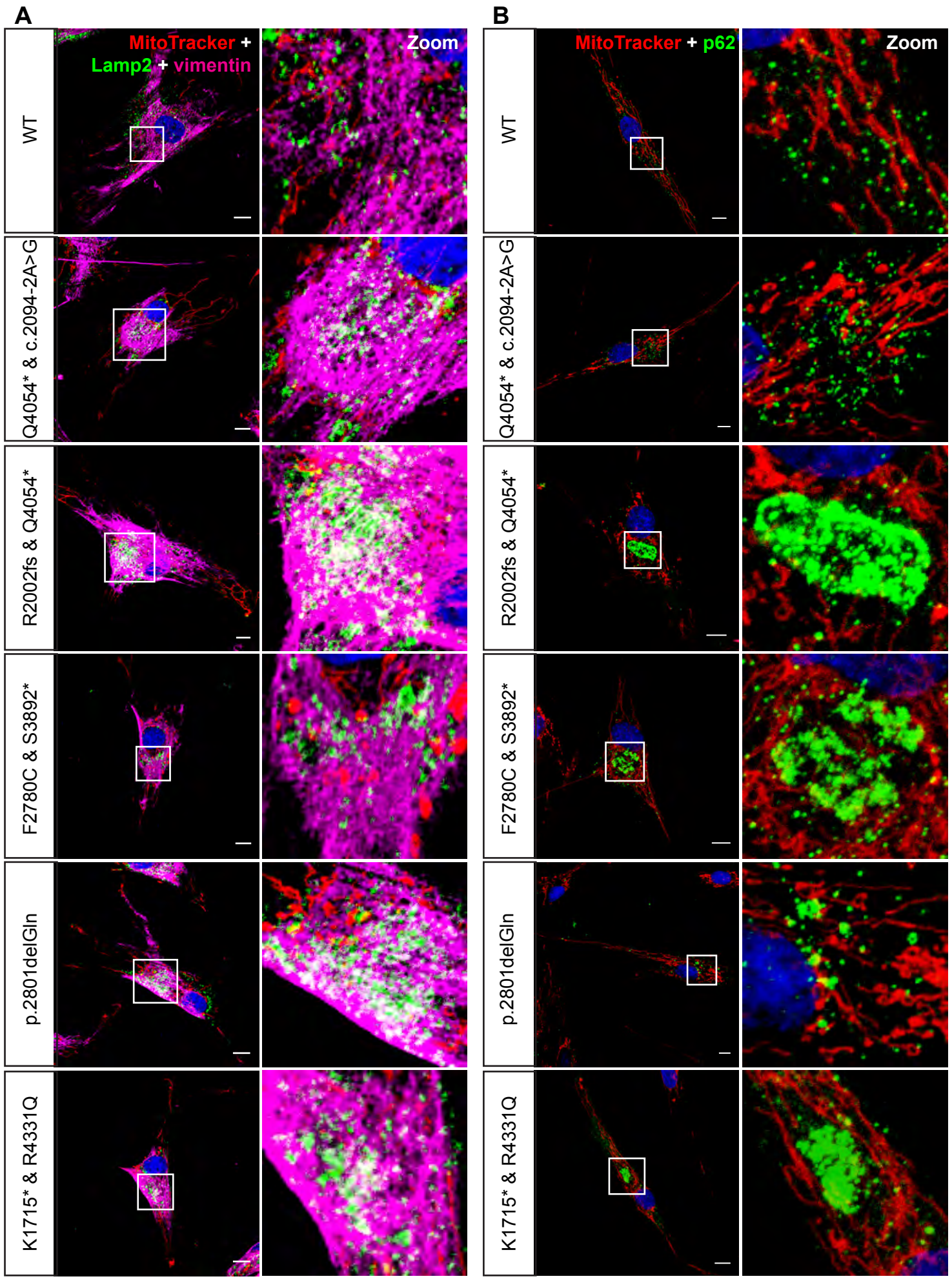

Figure S5. Accumulation of LAMP-2 and p62/SQSTM1 in ARSACS patient HDFs. (A) Representative confocal images of dermal fibroblasts from ARSACS patients or wild-type (WT) control. Cells were stained with 100μM MitoTracker for 30 minutes prior to fixation and permeabilisation. Cells were incubated with antibodies to **(A)** LAMP-2 and vimentin, or **(B)** p62/SQSTM1. Confocal analysis showed perinuclear accumulation of LAMP-2 and p62/SQSTM1 in ARSACS patient cells. White boxes in the merged panels are shown zoomed in the right-hand panels. Scale bars = 10 μm.